

# Flares in Open Clusters with K2.

## II. M35, Hyades, and Ruprecht 147

Ekaterina Ilin<sup>1</sup>, Sarah J. Schmidt<sup>1</sup>, Katja Poppenhäger<sup>1</sup>, James R. A. Davenport<sup>2</sup> and Klaus G. Strassmeier<sup>1</sup>

<sup>1</sup> Leibniz Institut für Astrophysik Potsdam

e-mail: eilin@aip.de

<sup>2</sup> University of Washington e-mail: jrad@uw.edu

Received XXX; accepted XXX

### ABSTRACT

**Context.** Flares can help us trace magnetic activity because are bright and high-contrast on low mass stars.

**Aims.** This study aims to quantify flaring activity on these stars as a function of mass and age.

**Methods.** We automatically detected flares in K2 time-domain photometry, using the open-source software K2SC to remove instrumental and astrophysical variability from K2 light curves. We used injection and recovery of synthetic flares to assess detection thresholds, time sampling and de-trending effects on the inferred flare energies. With additional data from the full K2 archive we added stars with a larger variety of ages and spectral types to the analysis of the previous study (Ilin et al. 2019). We compared previous results from the Pleiades and Praesepe to the flare frequency distributions (FFDs) in M35 and the Hyades, respectively. Ruprecht 147 filled in the age gap at 2.5 Gyr between the aforementioned young clusters and the solar age cluster M67.

**Results.** We find that the flare production mechanism is similar for the entire parameter space, following a power law relation with exponent  $\alpha \approx 2$ , but the flaring frequencies depend on both mass, and age. We discuss X and Y.

**Key words.** Methods: data analysis, Stars: activity, Stars: flare, Stars: low-mass

Use \titlerunning to supply a shorter title and/or \authorrunning to supply a shorter list of authors.

### 1. Introduction

Flares are explosions on stellar surfaces with a complex spatio-temporal and energetic phenomenology. We know that flares are magnetic re-connection events that lead to a change in field line topology and subsequent energy release (Priest & Forbes 2002). We can observe flares in nearly all electromagnetic bands, from radio to X-rays, and on all stars that possess a convection zone. From late F type stars to ultracool dwarfs (Gizis 2013). But even with continuous monitoring at high temporal resolution, the random occurrence of solar flares makes them costly observing targets, especially in coordinated multi-band observations. In integrated light, most solar flares have a far too low contrast and intensity to be observable. Stellar flares on cool stars have two advantages in this respect. They are often bright, enhancing stellar flux by up to several orders of magnitude, and they typically exhibit blackbody emission at temperatures significantly higher than their stars' photospheres. With the evidence that the physical processes that cause flares on the Sun and other stars are the same (Karoff 2016), solar and stellar flares can inform each other (Shibayama et al. 2013). Inconsistencies in extrapolations from solar to stellar conditions (Aarnio et al. 2011; Aarnio et al. 2012; Drake et al. 2012; Alvarado-Gómez et al. 2018). Large surveys like Kepler and TESS enable statistical flare studies of stars that were not pre-selected for their activity (Walkowicz et al. 2011). Statistical studies of stellar flaring activity can help us understand the underlying physical processes CITE stellar surface magnetic fields, starspots (Davenport 2015; Howard

et al. 2019b), how flares relate to stellar angular momentum evolution (Mondrik et al. 2019; Howard et al. 2019b), how they affect the atmospheres of exoplanets (Lecavelier des Etangs et al. 2012; Loyd et al. 2018; Tilley et al. 2019; Howard et al. 2019a), and inform galactic archaeology (Howard et al. 2019a).

Basic parameters that affect flaring behaviour on stars are their masses, and ages. Ages can be controlled for in coeval groups of stars, and flaring-age studies in binaries showed consistency in activity for both components in the majority of targets (Lurie et al. 2015; Clarke et al. 2018). Open clusters present other coeval groups of stars with well-determined ages. Ilin et al. (2019) (hereafter PaperI) investigated the flaring activity of late-K to mid-M dwarfs in three open clusters (OCs), the Pleiades, Praesepe, and M67, using K2 time domain photometry. They analysed the flare frequency distributions (FFDs), with respect to different masses and cluster ages. For the cluster members, the light curves revealed that their flaring activity declines both with age and mass. The decline is faster for higher mass stars. Recently, Davenport et al. (2019) put forward an empirical parametrization of this flaring-mass-age relation based on FFDs. The present study aims to extend the results in PaperI to the age of Ruprecht 147 (2.5 Gyr), and both higher and lower masses than in the previous study. We also test the previous results from the Pleiades on M35, and the results from Praesepe on the Hyades, as both OC pairs have approximately the same ages. Because the Kepler satellite retired in fall 2018, we can now use the complete K2 data set, and supplement all three OCs in PaperI with additional light curves. Additionally, we use high quality K2 light curves available for M67 (Nardiello et al. 2016) and M35 (Soares-Furtado et al. 2017). We discuss our results with

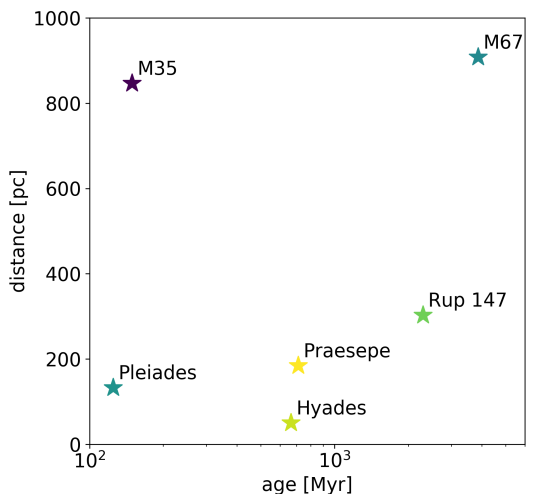


**Fig. 1.** The values for age, metallicity, and distance are approximate values from a compilation of existing literature, see Appendix B.1.

respect to potential breaks in the power law distribution at high energies. Finally, we use the results to test the parametrizability in Davenport et al. (2019).

## 2. Data

Our main data are K2 target pixel files that were provided by the Kepler archives hosted at MAST, and light curves derived from them (Aigrain et al. 2016; Soares-Furtado et al. 2017; Vinícius et al. 2018). To assign  $T_{\text{eff}}$  to the targeted stars we used multi-band photometry obtained from Tycho, UCAC4, 2MASS, Pan-STARRS, and Gaia catalogs. To assign ages to the targeted stars OC membership information was compiled from the literature. An overview over the cluster sample is presented in Table ?? and illustrated in Figure 1.

### 2.1. K2 light curves

The Kepler (Koch et al. 2010) spacecraft finished its follow-on mission K2 (Howell et al. 2014) in September 2018, after having completed nearly 20 80-day observing campaigns. Even though Kepler and K2 data are used in more than 2 400 publications to date, the public archive can still be considered understudied (Barentsen et al. 2018). In this spirit we took up the analysis of about 4 000 Kepler target pixel files that each contain up to 80 days of 30 min cadence observations in white light ( $4, 200 - 9, 000 \text{ \AA}$ ). We also used light curves extracted from the K2 C0 super stamp. A super stamp is an aggregated set of typical Kepler postage stamps placed over a densely populated field, that also covers M35 (Soares-Furtado et al. 2017).

As K2 was conducted on the two-wheeled Kepler satellite, it was subjected to substantial drift motion (spacecraft roll, Van Cleve et al. 2016) and had an overall reduced pointing accuracy. To mitigate these effects, various solutions were developed (Vanderburg & Johnson 2014; Aigrain et al. 2016; ?; Luger et al. 2018)

### 2.2. Membership matching

We obtained membership information from multiple catalogs for each cluster. We cross-matched these catalogs on RA and

declination within 3 arcsec. The resulting target lists were used to search the K2 archive, or were matched to the catalogs of extracted light curves from crowded fields in the case of M35 (Soares-Furtado et al. 2017) and M67 (Nardiello et al. 2016).

One part of the membership catalogs provided membership probabilities (Douglas et al. 2014; Bouy et al. 2015; Cantat-Gaudin et al. 2018; Olivares et al. 2018; Reino et al. 2018; Gao 2018; Olivares et al. 2019). For the other part no probability was provided (Rebull et al. 2016a; Douglas et al. 2017; Gaia Collaboration et al. 2018a), or qualitative classifiers were given (Curtis et al. 2013; Gonzalez 2016; Rebull et al. 2017). In the latter cases we assigned approximate probabilities anchored to the set threshold for inclusion into our final sample. Absence in a catalog did not decrease the likelihood of membership, as each catalog shows different selection biases which we did not address in this study. We set the threshold mean membership probability  $p$  for a target in our sample to 0.8.

## 2.3. Open Clusters

We studied flaring activity in the low mass stars in six open clusters spanning from ZAMS to solar age. Table 1 provides an overview over the final sample. The literature overview of age, distance, and metallicity determinations is given in Table ?? in the Appendix. Membership probability histograms of the final sample are displayed in Figure ??.

### 2.3.1. Pleiades

The Pleiades, a nearby ZAMS cluster, were observed in Campaign 4, and were treated in PaperI. We include the cluster in this work for completeness and to illustrate improvements to (PaperI). We revisited the memberships from Rebull et al. (2016a), which were your in the previous work, and merged them with lists of members determined by Olivares et al. (2018); Gaia Collaboration et al. (2018a); and Cantat-Gaudin et al. (2018).

### 2.3.2. M35

M35 is a ZAMS cluster 900 pc away, observed during Campaign 0 in K2. We merged membership lists from Cantat-Gaudin et al. (2018); Gaia Collaboration et al. (2018a); and Bouy et al. (2015). There are only five K2 light curves, but we identified multiple additional members with publicly available<sup>1</sup> light curves obtained from Soares-Furtado et al. (2017). They used an image subtraction technique in the campaign's super stamps, a self flat-fielding de-trending inspired by K2SFF (Vanderburg & Johnson 2014), and a trend-filtering algorithm developed by Kovács et al. (2005). We preferred PSF photometry in cases where both aperture K2 and PSF LCs were available. We took the raw extracted PSF light curves and de-trended them using K2SC.

### 2.3.3. Hyades

The Hyades are a 0.6 Gyr old OC observed during Campaigns 4 and 13 with K2. It is about as old as Praesepe. We merged membership tables obtained from Douglas et al. (2014); Reino et al. (2018); and Gaia Collaboration et al. (2018a).

<sup>1</sup> <https://k2.hatsurveys.org/archive/>

**Table 1.** Open clusters.

cluster	<i>n</i>	LCs	SLCs	LLCs	PSF LCs	age[Myr]	distance[pc]	[Fe/H]
Pleiades	2033	944	33	911	0	125		
M35	1614	5	0	5	158			
Hyades	655	301	42	259	0			
Praesepe	1281	2500	68	2432	0			
Rup 147	213	97	25	72	0			
M67	1344	1141	118	1023	1019			

**Notes.** *n* is the approximate number of members with  $p > 0.8$ . LCs, SLCs, LLCs, and PSF LCs denote the number of available light curves, short cadence light curves, long cadence light curves, and PSF de-detrended light curves, respectively. The values for age, [Fe/H], and distance are approximate values from a comparison of existing literature, detailed in Appendix B.1.

#### 149 2.3.4. Praesepe

150 Praesepe appeared in Campaign 5, and was previously treated  
151 in PaperI. It was then observed again during Campaign 13. We  
152 revisited the memberships obtained by Douglas et al. (2014), and  
153 matched them to the members identified in Douglas et al. (2017)  
154 Rebull et al. (2017); Cantat-Gaudin et al. (2018); and Gaia Col-  
155 laboration et al. (2018a).

191 used the average extinction value of the respective cluster. We  
192 accounted for extinction in Gaia BP and RP using the reddening  
193  $E(B_P - R_P)$  derived from Gaia photometry and parallax from  
194 Gaia DR2 (Andrae et al. 2018). We dropped targets that were  
195 too bright (Kepler magnitude  $K_p \leq 9$ ).  
196

#### 197 2.3.5. Ruprecht 147

198 Ruprecht 147 is a 2.5 Gyr old OC observed during Campaign 5  
199 with K2. We used the mean membership probabilities obtained  
200 from a number of studies (Curtis et al. 2013; Cantat-Gaudin et al.  
201 2018; Olivares et al. 2019) combined with the members found  
202 by Gaia Collaboration et al. (2018a) to identify the most likely  
203 members.

#### 204 2.4.2. Effective temperatures

#### 205 2.3.6. M67

206 M67 is a solar-age, solar metallicity OC about 900 pc away.  
207 Multiple members were observed during Campaign 5, and 208 visited in Campaigns 16 and 18. We did not find any flares 209 in M67 in Campaign 5 (PaperI) observing the members identified  
210 by Gonzalez (2016). The recent campaigns brought both ad-211  
212 tional observations, and entirely new targets to the sample. We  
213 merged the members from Gonzalez (2016) with a recent study  
214 based of Gaia DR2 data (Gao 2018). Additionally, we obtained  
215 PSF-detrended light curves for Campaign 5 from Nardiello et al.  
216 (2016).

217 We applied several methods and color-temperature relations  
218 (CTRs) to determine robust  $T_{\text{eff}}$ . We used CTRs from Boyajian et al. (2013) and Mann et al. (2016) (erratum to Mann et al. 219 2015), and  $T_{\text{eff}}$  derived from Gaia DR2 using the StarHorse algorithm (Queiroz et al. 2018) and inferred from Gaia DR2 using the Apsis pipeline (Bailer-Jones et al. 2013; Andrae et al. 2018).  
220 Boyajian et al. (2013) determined CTRs from a range of inter-221  
222 ferometrically characterized stars using  $g - z$ ,  $g - i$ ,  $g - r$ ,  
223  $g - J$ ,  $g - H$ , and  $g - K$  colors from SDSS and Johnson magni-224  
225 tudes for A to K stars. Their sample is centered on solar metal-226  
227 licity, so we constrained the use of these CTRs to stars with  
228  $-0.25 < [\text{Fe}/\text{H}] < 0.25$ . We transformed 2MASS JHK to  $J - H$ ,  
229  $H - K$ , and  $J - K$  in the Johnson system as the authors from  
230 2MASS to the Bessell-Brett system (Carpenter 2001), and from  
231 Bessell-Brett to Johnson using the relations in Bessell & Brett  
232 (1988).

233 Mann et al. (2015) provide CTRs from absolutely calibrated  
234 spectra to which they fitted atmospheric models to obtain  $T_{\text{eff}}$ .  
235 Alternatively, they determined  $T_{\text{eff}}$  from long-baseline optical  
236 interferometry measurements using the bolometric flux. Among  
237 others, they note transformations for SDSS/2MASS  $r - z$  and  
238  $r - J$ , or Gaia  $BP - RP$  where extra information can be added  
239 from metallicity or 2MASS  $J - H$ . The relations in Mann et al.  
240 (2015) are only valid if metallicity is sufficiently close to solar,  
241 which is satisfied for all clusters in this paper (see Table ??).  
242 M35 may be an exception to this rule.

243 We supplemented our estimates with  $T_{\text{eff}}$  estimates from Anders  
244 et al. (2019) who used the StarHorse pipeline (Queiroz et al.  
245 2018) on Gaia DR2.

246 Gaia DR2 published effective temperatures for over 160 million  
247 sources (Gaia Collaboration et al. 2018b). The typical uncer-  
248 tainty is quoted at 324 K, but it is lower for stars above  $\sim 4100$   
249 K and below  $\sim 6700$  K, so that we adopt 175 K which is above  
250 the quoted root-median-squared error in this  $T_{\text{eff}}$  range (Andrae  
251 et al. 2018), and use provided values only in this range.

252 Empirical CTRs suffer from systematic errors that stem both  
253 from the different methods applied, and from sample selection  
254 biases. We used as many empirical relations as possible in their  
255 appropriate ranges to obtain multiple  $T_{\text{eff}}$  estimates from which  
256 we then drew a more reliable median value. Targets that were  
257

#### 258 2.4. Effective temperatures, stellar radii, and luminosities

##### 259 2.4.1. Photometry and extinction correction

260 We determined effective temperatures  $T_{\text{eff}}$  using broadband  
261 photometry the Two Micron All Sky Survey (2MASS; Skrutskie  
262 et al. 2006), the Panoramic Survey Telescope and Rapid  
263 Response System (Pan-STARRS) Data Release 1 (Chambers et al.  
264 2016), and Gaia DR2 (Gaia Collaboration et al. 2018b). We  
265 applied quality cuts to 2MASS, Pan-STARRS DR1, and Gaia DR2  
266 data, as described in Appendix C, and removed foreground  
267 stars using Gaia DR2 parallaxes. We corrected the 2MASS  
268 and PanSTARRS photometry in M35, M67, and Ruprecht  
269 147 for extinction using the most recent version (Green et al.  
270 2019) of the dustmaps package that provides 3D dust maps  
271 derived from 2MASS and PanSTARRS photometry together  
272 with Gaia distances (Green et al. 2018). If there was no  
273 parallax available we used the cluster median distance instead.  
274 If an extinction value was not available for a given star  
275

lacking sufficient photometric data to derive  $T_{\text{eff}}$ , or were too hot to be expected to have a convective envelope ( $T_{\text{eff}} \geq 7000$  K), were flagged accordingly, and removed from the sample. We dropped all targets where the uncertainty on the weighted mean  $T_{\text{eff}}$  was greater than 10%. Only targets that were assigned a  $T_{\text{eff}}$  were searched for flares.

#### 2.4.3. Stellar radii

We used a catalog of empirically characterised stars (Yee et al. 2017) to derive  $R_*$  from  $T_{\text{eff}}$  (Fig. 4). Yee et al. (2017) collected 404 stars with high-resolution spectra from the literature, and own observations of mid to late K-dwarfs, spanning low mass stars from 7000 K down to 3000 K. For these stars, the resulting catalog is accurate to 100 K in  $T_{\text{eff}}$ , 15 % in  $R_*$ , and 0.09 dex in [Fe/H]. We interpolated between stars from the catalog to our derived  $T_{\text{eff}}$ , and propagated the resulting scatter to the uncertainty in  $R_*$  if  $T_{\text{eff}} > 3500$  K. For stars with  $T_{\text{eff}} < 3500$  K we used  $T_{\text{eff}} - R_*$  relations derived by (Mann et al. 2015, 2016).

#### 2.4.4. Spectra

We assigned spectra to our targets from the SpecMatchEmp Yee et al. (2017) and the FlareSpecPhot libraries (Schmidt 2014; Kirkpatrick et al. 2010; Burgasser et al. 2007, 2008, 2010, 2004; Cruz et al. 2004; Burgasser & McElwain 2006; Rayner et al. 2009; Doi et al. 2010; Filippazzo et al. 2015; Cruz et al. 2003; West et al. 2011; Bochanski et al. 2010, 2007; Schmidt et al. 2010, 2015, 2014; Mann et al. 2015). When a spectrum was available for the derived spectral type in FlareSpecPhot, we preferred it over SpecMatchEmp, which was the case for all stars cooler than M0, where we mapped spectral type to effective temperature as appears in Pecaut & Mamajek (2013). We then combined stellar radii  $R_*$ ,  $T_{\text{eff}}$ , and spectra to projected bolometric luminosities  $L_{\text{bol},*}$ , and projected luminosities in the Kepler band  $L_{\text{Kp},*}$  (Shibayama et al. 2013; Ilin et al. 2019). Uncertainties  $L_{\text{Kp},*}$  ranged from 9 % to 52 % with a median value of 17 %.<sup>294</sup>

### 3. Methods

We detected flare candidates automatically, and validated the by eye. We attempted to assign recovery probabilities and corrected for sampling effects using injection/recovery tests but the procedure was not scalable due to computational costs. We performed injection recovery on a handful of example light curves to see that de-trending and intrinsic light curve properties smear out the  $ED$  recovery with varying distributions that add an uncertainty of about 30%. Most of the candidates are expected to have a complex shape that deviates from the classical flare template. The validation yielded an estimate on the uncertainty on the energy released in the Kepler band. The frequency distribution of these flare energies are believed to follow a power law that spans multiple orders of magnitude. We adopted this model, and used two different Maximum Likelihood estimators to obtain the power law exponents. We tested the best fit parameters with the Kolmogorov-Smirnov test, and probed possible truncation of the power law relation with an exceedance test.

#### 3.1. Flare finding

We used the open source software AltaiPony<sup>2</sup> to automatically detect and characterize flares in our sample. The code base

lies on K2SC<sup>3</sup> (Aigrain et al. 2016) to remove instrumental and astrophysical variability from K2 light curves. We did not use the pre-detrended light curves available on MAST, but used K2SC to derive our own, because we clipped outliers at  $3\sigma$  iteratively, as compared to the original work, where outliers were clipped at  $5\sigma$  (Aigrain et al. 2016).

After de-trending, the flare finder algorithm looked for continuous observing periods, defined as being longer than 10 data points at a minimum cadence of 2 h. All further routines were run on these observing periods. The finder iteratively clipped excursions from the median value at  $3\sigma$  rolling window noise above median plus uncertainty given from K2SC de-trending. After each iteration, outliers were cut down to the current median value. Either after convergence, or 50 iterations, the resulting median value was adopted. With this median as quiescent flux, flare candidates were identified with the same procedure as during the median value calculation, but now we additionally required at least three consecutive data points to fulfil the  $\sigma$ -criterion. Flare candidates were merged into single candidate events if they were no more than three data points apart. For each of these candidates occurrence time, amplitude and equivalent duration ( $ED$ ) was returned.

The Kepler flare sample has shown to be difficult to treat in a fully automated way. Without manual vetting, the event samples remain significantly contaminated (Yang & Liu 2019).

$ED$  is the area between the LC and the quiescent flux, that is, the integrated flare flux divided by the median quiescent flux  $F_0$  of the star, integrated over the flare duration (Hunt-Walker et al. 2012):

$$ED = \int dt \frac{F_{\text{flare}}(t)}{F_0}. \quad (1)$$

$ED$  is a quantity independent of calibration and distance that is suited to compare flaring activity on stars where these properties are uncertain. It describes the time during which a star releases as much energy as the flare itself. This time can be shorter or longer than the actual flare duration.

The uncertainty in  $ED$  depends on the light curve noise properties, time sampling, and other intrinsic characteristics. Moreover, K2SC de-trending and the flare finding procedure introduce additional uncertainty that dominates the photometric noise. Carrying out injection and recovery that takes into account the effect of GP regression that underlies K2SC. We only performed injection-recovery on a small number of light curves with flares to estimate the .

#### 3.2. Kepler flare energies

(see PaperI for details).

Multiband time resolved observations of active M dwarfs have shown that continuum flux accounts for the majority of the energy radiated by flares (Kowalski et al. 2013). The effective temperature of this blackbody, however, varies by a great degree, with, to date, no robust predictor of that temperature:

While solar flares are relatively cool, with  $T_{\text{eff}} \approx 5000 - 7000$  K (Kleint et al. 2016; Kerr & Fletcher 2014; Watanabe et al. 2013; Namekata et al. 2017), at least one M dwarf flare reached 40 000 K as seen in FUV spectra (Froning et al. 2019), and most events exhibit temperatures of about 9 000 – 10 000 K (Hawley & Fisher 1992; Kretzschmar 2011; Shibayama et al. 2013). A dependence of flare temperature on stellar age, or mass, or both, will enter our analysis if we attempt

<sup>2</sup> <https://github.com/ekaterinailin/AltaiPony>

<sup>3</sup> <https://github.com/OxEs/k2sc>

318 to quantify bolometric flare energy. At about 6 200 K, the Kepler  
 319 pass band captures the largest flux fraction, at 10 000 K 72%  
 320 at 40 000 K only 4% of this value is transmitted. Another effect  
 321 is that flares of equal flare energy but hotter SED would not be  
 322 seen in the Kepler band at all.  
 323 We propagated the uncertainties  $\sigma_{ED}$  and  $\sigma_L$  (on  $L_{*,Kp}$ )  
 324 quadrature to  $E_{Kp,\text{flare}}$ .  
 325

### 326 3.3. Power law fits

327 Flare frequency distributions follow power law relations that  
 328 cover several orders of magnitude, from solar microflares to stellar  
 329 superflares. We fitted power law functions to the FFDs using  
 330 three different approaches.  
 331 The first method was a maximum likelihood estimator (MLE) (Maschberger & Kroupa 2009). As recommended by Maschberger & Kroupa (2009), we applied the stabilized Kolmogorov-Smirnov (KS) test at 95 % significance level to all power law fits in the sample. If the test fails the power law model does not fit the data at the given significance level. If the test passes, this does not give any information whether the power law model is the correct assumption. The goodness of fit can be estimated from the visual inspection of percentile-percentile plots, given in the online material<sup>4</sup>. We used the KS test iteratively to determine the FFDs' low-energy cutoff  $ED_{\min}$ .  
 342 The second method used the MLE result as a prior for  $\alpha$ . Following Wheatland (2004), we defined the joint posterior distribution for the probability  $\epsilon$  that a flare with  $ED$  or energy above some value  $S_2$  occurs within a time period  $\Delta T$ :

$$p(\epsilon, \alpha) = C \cdot (-\ln(1 - \epsilon))^M \cdot (\alpha - 1)^M \cdot \Gamma(\alpha) \left[ \frac{(S_2/S_1)^{M+1}}{\pi} \right]^\alpha \cdot (1 - \epsilon)^{(T/\Delta T) \cdot (S_2/S_1)^{\alpha-1} - 1}. \quad (2)$$

346  $C$  is the normalisation constant,  $M$  is the number of events,  $T$  the total observation time.  $\Gamma$  contains the prior distribution for  $\alpha$ ,  
 347 and  $S_1$  denotes the detection threshold above which all flares  
 348 detected.  $\pi$  encapsulates the flare energies as

$$\pi = \prod_{i=1}^M \frac{s_i}{S_1}$$

349 , where  $\{s_1, s_2, \dots, s_m\}$  are the flare energies or  $ED$ .  
 350 The posterior distribution in Wheatland (2004) captures both  
 351 the Poissonian distribution of flare events in time, and their  
 352 power law distribution in energy, simultaneously. Wheatland  
 353 (2004) derived this model to be able to predict the flaring rate of  
 354 a given active region on the sun, and offered an extension to Eq.  
 355 2 that treated changing flaring activity rates as the active region  
 356 evolves, and also characteristics of the active region itself, such  
 357 as sunspot classifiers. In our simplification of the model, we  
 358 assumed that the flare generating process did not change within  
 359 the observation time span in any star in our sample ( $M = M^{414}$   
 360 Eq. 24 in Wheatland (2004)). Another assumption was that this  
 361 process was the same for all stars in the sample ( $\Lambda_{MC} = \Lambda_{MC}^{415}$   
 362 Eq. 24). Under these assumptions the information gained from the  
 363 light curves could be stacked together.  
 364 With a uniform prior for  $\alpha$  the results from the MLE and Markov  
 365

366 Chain Monte Carlo (MCMC) sampling from the posterior distribution are the same, the latter allowed us to fit for  $\epsilon$  and  $\alpha$  simultaneously. Another advantage of the latter approach is that we could use more informative priors. We also used a Gaussian fit to  $\alpha$  obtained from the posterior distribution using the full sample of flares as the prior for a subsequent Bayesian analysis of individual age and  $T_{\text{eff}}$  bins. Assuming that  $\alpha$  is universal for all spectral types, ages, and flare energy ranges, we used this more informative, Gaussian prior to further constrain the flaring rates.

367 Additionally we calculated the exceedance statistic  $tr$  to test if the power law distribution was truncated. If  $tr$  is 1, the power law distribution is truncated at the high energy end. If  $tr$  is 0, no information was gained from the calculation. To derive  $tr$ , given a number  $n$  of observations  $X_n$  and a best fit value for the power law exponent, we generated 500 samples with  $n$  values from this best-fit distribution assuming no truncation, i.e. choosing an upper limit several orders of magnitude higher than  $X_{max}$ . We then proceeded to truncate the samples at thresholds  $T$  below the maximum observed value  $X_{max}$  and determined the average number  $N_{ex}$  of generated values that will exceed  $T$ . If the underlying power law is not truncated,  $N_{ex}$  declines with larger  $n$ , as larger  $X_{max}$  will be present in the original data. If the best fit power law exponent is steeper,  $N_{ex}$  will be underestimated. If the best fit power law exponent is flatter,  $N_{ex}$  will be overestimated. If the power law is not truncated, for  $n \geq 100$   $N_{ex}/n$  will be  $< 5\%$ , for  $20 < n < 100$ , typically  $N_{ex}/n < 15\%$ .

## 395 4. Results

396 Fig. ?? shows the  $E_{Kp,\text{flare}}$  and  $ED$  detection thresholds, as defined by the recovery probability (see Sec. ??). The thresholds in  $ED$  reflect the noise level in the light curves.

### 4.1. Flaring activity as a function of age and $T_{\text{eff}}$

401 Flaring activity decays with age. Flaring fraction was observed to decline with galactic latitude for M dwarfs (Hilton et al.  
 402 2010) Howard+2019. Short rotation periods and high magnetic  
 403 activity measured in H $\alpha$  are strongly correlated (West et al.  
 404 2015). According to gyrochronology, fast rotation indicates  
 405 young age (Barnes 2003), and slows down as the star ages. Here,  
 406 we quantify how this decline unfolds for different spectral types.  
 407 Except for the stars in our coolest temperature bin (M5.5-M8,  
 408 2 500-3 000 K), stellar flaring activity at a given age is always  
 409 stronger for a cooler star. The exception is seen at cluster ages  
 410 around 120 Myr.

411 What creates the strong emission in white light? Extended flare  
 412 loops, maybe (?)

### 4.2. M67

413 We found one very likely flare candidate in the PSF-detrended  
 414 light curves (Nardiello et al. 2016). After having searched the  
 415 entire sample we identified about 250 candidates. We excluded  
 416 those candidates that clustered spatio-temporally in different  
 417 light curves as systematics. After vetting the remaining 25 by  
 418 eye, we excluded false positives judging by their morphology,  
 419 leaving a mere ten light curves with flare-like shape. One target  
 420 appeared to be an echo from one of the other light curves.  
 421 Five targets were foreground stars, two are more likely back-  
 422

<sup>4</sup> <https://github.com/ekaterinailin/flare-in-clusters-with-k2-ii>

423 ground stars, one target is probably a giant and does not appear  
 424 in Gaia photometry (IR source). Only one target (Gaia DR2  
 425 604922435422864512) appears to reside at M67 distance and is  
 426 a  $p = 0.997$  member according to Gao (2018). Our estimates  
 427 indicate that it is a M2V. If the spectral class is correct, the flare  
 428 releases about  $6.1 \cdot 10^{33}$  erg ( $ED = 1391 \pm 548$  s) in the Kepler  
 429 band.

### 430 4.3. Flaring Activity Indicators

431 Flaring rates:  $FR$  and flaring fraction We define  $FR$  as the flare  
 432 rate above detection thresholds on  $E_{Kp,\text{flare}}$  and  $ED$  in each  $T_{\text{eff}}$   
 433 bin, respectively (Figs. ?? and ??).

434 Flaring energy:  $FA$  and  $L_{Kp,\text{flare}}$  The energy released in flares  
 435 was inferred using our derived stellar luminosities. It declines  
 436 with age for every  $T_{\text{eff}}$  bin considered for both the total luminosity  
 437 and relative to the quiescent flux (Fig. ??).  
 438

439  $L_{Kp,\text{flare}}$  is the luminosity in flares in the Kepler band. We can relate  
 440 this to the quiescent bolometric luminosity of the star where  
 441 we define the fractional flare luminosity  $FA$  as in PaperI:  
 442

$$443 FA = \frac{1}{N} \sum_i^N FA_i = \frac{1}{N} \sum_i^N \frac{E_{Kp,\text{flare,tot},i}}{t_i \cdot L_{\text{bol},*,i}}$$

444 We determine  $L_{\text{bol},*}$  from  $R_*$  and  $T_{\text{eff}}$ , as described in Sec. 2.4.  
 445 This is a meaningful measure of relative stellar activity as long  
 446 as only the flux portion of the quiescent star in the Kepler band is  
 447 roughly constant. It is therefore sensible to compare  $FA$  values  
 448 across ages, but not across  $T_{\text{eff}}$ .  
 449

450 FFD Power law fit parameters to the FFDs (Figs. 5 and 6) are  
 451 sensitive to the low-energy cutoff, where most observations are  
 452 side. The goodness of fit strongly depends on the sample size.  
 453 Power law fit parameters derived using MLEs, as described in  
 454 Sec. 3.3, are mostly consistent with each other but often deviate  
 455 from  $\alpha = 2$ . A smaller sample size tends to create a flatter  
 456 distribution (Figs. 7 and 8). Truncation was not detected for FFDs  
 457 with more than 50 flares (Tables 2 and 3) For these results, ex-  
 458 trapolations outside of the observed energy range are clearly off.  
 459 If we assume  $\alpha \equiv 2$ , different distributions can be compared. For  
 460 fixed  $\alpha$ , in the  $ED$  domain,  $\beta_2$  is the flare frequency at  $ED = 504$   
 461 and shows a trend in both  $T_{\text{eff}}$ , and age (see Fig. ??). In the energy  
 462 domain, the picture is less clear (Fig. ??).  
 463

464 Compare to other FFD values, e.g., from Ward's Evryscope survey,  
 465 see table in Appendix, and maybe convert it to a plot Howard et al  
 466 (2019) monitored superflares on cool stars with bolometric  
 467 energies above  $10^{33}$  erg and up to  $10^{36}$  erg. They find power law  
 468 exponent values around  $\sim 2$  resolved by spectral types. Similar  
 469 values are found for individual flare stars (Lurie et al. 2015).  
 470 Howard+18, Loyd+18, Tilley+19 show that flares can erode  
 471 oplanetary atmospheres. If a flare is assumed to deposit its  
 472 energy in an instant a single superflare can completely remove  
 473 the ozone layer at the substellar point Loyd+18. Associated  
 474 tons are safer way to ozone destruction if they are associated  
 475 with reoccurring large flares Tilley+19  
 476

## 477 5. Discussion

### 478 5.1. Consistency with other studies

479 EvryFlare, mass-dependence,

### 480 5.2. Flaring and rotation

481 More energetic flares can be expected from faster rotating  
 482 stars (Candelaresi et al. 2014; Doorslaere et al. 2017; Yang  
 483 et al. 2017). Findings that flares with intermediate Rossby num-  
 484 ber appear to flare more than fast and slow rotators (Mondrik  
 485 et al. 2019) could not be reproduced here or in the EvryFlare  
 486 survey (Howard et al. 2019b). If enhanced flaring can be inter-  
 487 preted as an increase in the stellar angular momentum loss rate  
 488 flaring activity can be used to inform the cause of variation in the  
 489 spin-down efficiency. An example of such variations is the appar-  
 490 ent temporary stalling of spin-down seen in K dwarfs in NGC  
 491 6811 (Curtis+2019). The authors favored a scenario in which  
 492 the stellar core transfers momentum onto the envelope but did  
 493 not rule out the possibility of a decreased magnetic braking effi-  
 494 ciency. In the latter scenario, these stars should flare less.  
 495

496 We used rotation periods derived from K2 light curves for the  
 497 Pleiades (Rebull et al. 2016b), the Hyades (Douglas et al. 2016),  
 498 and Praesepe (Rebull et al. 2017), to illuminate the rotation-  
 499 flaring relation at fixed ages. In the Pleiades, most flaring stars  
 500 are found on the fast rotator branch at or below one day, and  
 501 flaring activity peaks in this regime. For Praesepe, flaring rates  
 502 appear to ... In the Hyades, all of the 11 stars with rotation  
 503 periods that overlapped with our sample were found flaring, but  
 504 the number were too low to provide statistical insight. For Rup  
 505 147, M35 and M67, no rotation rates were available at the time.

### 506 5.3. M37

507 Comparing our results to a similar study of photometric flares  
 508 in M37 (Chang et al. 2015) we find the results somewhat dis-  
 509 crepant. M37 is 300-600 Myr old and appears less active than  
 510 Praesepe and Hyades in individual Teff bins, which are of coeval  
 511 or older. We attribute the difference to the loose membership re-  
 512 quirement of  $pmem \geq 0.2$  in Chang et al. (2015) as compared to  
 513 our stricter cuts at 0.8. We expect the M37 to be contaminated  
 514 with field stars that systematically reduce the flaring rates. Ap-  
 515 plying our own restriction the M37 sample (Chang et al. 2016)  
 516 leaves very few flares that hamper a statistical description of their  
 517 distributions.

### 518 5.4. Division at 3000 K

519 The lowest  $T_{\text{eff}}$  bin at Pleiades age in our sample reflects the  
 520 division between fully convective stars and those with a radi-  
 521 ative core (Reid & Hawley 2005). At this age, the coolest dwarfs  
 522 may still be accreting angular momentum on the PMS, instead  
 523 of spinning down on the MS. We suggest that a regime change  
 524 occurs around 120 Myr for stars with  $T_{\text{eff}} = 2500 - 3250$  K.  
 525 Below 3000 K, an analysis of 66 ZDI maps show that magnetic  
 526 field configurations can be strong and dipolar or weak and multi-  
 527 polar (Morin et al. 2008; See et al. 2017). If these stars can be  
 528 distinguished by age, this should be reflected in our age-resolved  
 529 flaring activity. If the difference is not a function of age, we  
 530 should see a similar bimodal distribution of very inactive and  
 531 very active stars in the lowest mass bins. If the difference be-  
 532 tween the two configurations is a function of age, we should only  
 533 see one type of stars with correspondingly similar behaviour in  
 534 these  $T_{\text{eff}}$  bins.

535 The lowest mass bin appears underactive compared to the rest of  
 536 the flaring-age- $T_{\text{eff}}$  relation in the  $ED$  domain. Physical explana-  
 537 tions for this peculiarity include: A different magnetic structure  
 538 A truncation of the power law that reflects the maximum  $ED$  an  
 539 active region can produce on these stars.

**Table 2.** Summary of activity parameters of all clusters and  $T_{\text{eff}}$  bins in energy distributions.

cluster	$T_{\min}$ [K]	$T_{\max}$ [K]	$n_*$	$n_{\text{flares}}$	age [Myr]	[Fe/H]	$E_{\text{Kp,flare,min}}$ [erg]	$\sigma_B$	$\alpha_{\text{MK}}$	$\beta_2$ [ $\text{yr}^{-1}$ ]	$\beta_B$ [ $\text{yr}^{-1}$ ]	$\beta_{\text{MK}}$ [ $\text{yr}^{-1}$ ]	$tr_2$	$tb_{\text{B}}$	$tr_{\text{MK}}$
Pleiades	4000	4999	87	148	125 $\pm^{25}_{25}$	-0.02 $\pm 0.03$	1 $\cdot 10^{34}$	1.70 $\pm 0.24$	1.58 $\pm 0.20$	7.19 $\cdot 10^{33}\pm 2.32 \cdot 10^{32}$	2.07 $\cdot 10^{23}\pm 5.12 \cdot 10^{22}$	1.39 $\cdot 10^{19}\pm 2.87 \cdot 10^{18}$	0	James R.	0
Pleiades	3000	3249	353	420	125 $\pm^{25}_{25}$	-0.02 $\pm 0.03$	4.6 $\cdot 10^{33}$	-	1.35 $\pm 0.42$	6.57 $\cdot 10^{32}\pm 1.60 \cdot 10^{31}$	-	1.09 $\cdot 10^{10}\pm 4.74 \cdot 10^9$	0	0	0
Pleiades	3250	3499	168	324	125 $\pm^{25}_{25}$	-0.02 $\pm 0.03$	4.8 $\cdot 10^{32}$	2.08 $\pm 0.12$	2.06 $\pm 0.11$	1.71 $\cdot 10^{33}\pm 6.95 \cdot 10^{30}$	8.03 $\cdot 10^{35}\pm 9.34 \cdot 10^{34}$	1.97 $\cdot 10^{35}\pm 2.25 \cdot 10^{34}$	0	R. A.	0
Pleiades	3750	3999	52	92	125 $\pm^{25}_{25}$	-0.02 $\pm 0.03$	5.2 $\cdot 10^{32}$	1.86 $\pm 0.12$	1.83 $\pm 0.11$	4.01 $\cdot 10^{33}\pm 4.99 \cdot 10^{31}$	7.09 $\cdot 10^{28}\pm 8.49 \cdot 10^{27}$	8.29 $\cdot 10^{27}\pm 9.52 \cdot 10^{26}$	0	Davenport and Klaus G.	0
Pleiades	5000	5999	53	23	125 $\pm^{25}_{25}$	-0.02 $\pm 0.03$	3.7 $\cdot 10^{32}$	-	1.28 $\pm 0.31$	1.51 $\cdot 10^{33}\pm 1.56 \cdot 10^{32}$	-	1.66 $\cdot 10^{8}\pm 5.19 \cdot 10^7$	0	0	0
Pleiades	3500	3749	50	127	125 $\pm^{25}_{25}$	-0.02 $\pm 0.03$	3.8 $\cdot 10^{32}$	1.74 $\pm 0.09$	1.72 $\pm 0.09$	4.44 $\cdot 10^{33}\pm 8.32 \cdot 10^{31}$	7.47 $\cdot 10^{24}\pm 6.80 \cdot 10^{23}$	1.93 $\cdot 10^{24}\pm 1.70 \cdot 10^{23}$	0	0	0
M35	4000	4999	216	23	149 $\pm^{23}_{23}$	-0.21 $\pm 0.06$	1.6 $\cdot 10^{33}$	1.23 $\pm 0.32$	1.24 $\pm 0.27$	3.15 $\cdot 10^{35}\pm 5.31 \cdot 10^{32}$	2.20 $\cdot 10^6\pm 7.14 \cdot 10^5$	4.81 $\cdot 10^6\pm 1.34 \cdot 10^6$	0	1	1
Hyades	4000	4999	32	24	665 $\pm^{13}_{13}$	0.13 $\pm 0.01$	1.2 $\cdot 10^{32}$	-	1.06 $\pm 0.14$	8.40 $\cdot 10^{32}\pm 1.54 \cdot 10^{32}$	-	1.07 $\cdot 10^9\pm 1.83 \cdot 10^8$	0	0	1
Hyades	3000	3249	54	115	665 $\pm^{13}_{13}$	0.13 $\pm 0.01$	2.5 $\cdot 10^{32}$	1.89 $\pm 0.18$	1.85 $\pm 0.17$	1.15 $\cdot 10^{33}\pm 6.45 \cdot 10^{30}$	1.93 $\cdot 10^{29}\pm 3.51 \cdot 10^{28}$	1.33 $\cdot 10^{28}\pm 2.28 \cdot 10^{27}$	0	0	0
Hyades	3250	3499	42	140	665 $\pm^{13}_{13}$	0.13 $\pm 0.01$	2.2 $\cdot 10^{33}$	2.09 $\pm 0.65$	1.90 $\pm 0.47$	2.19 $\cdot 10^{33}\pm 9.70 \cdot 10^{31}$	2.06 $\cdot 10^{36}\pm 1.33 \cdot 10^{36}$	1.13 $\cdot 10^{30}\pm 5.36 \cdot 10^{29}$	0	0	0
Hyades	3750	3999	5	25	665 $\pm^{13}_{13}$	0.13 $\pm 0.01$	6.3 $\cdot 10^{31}$	1.47 $\pm 0.23$	1.45 $\pm 0.19$	2.12 $\cdot 10^{33}\pm 9.71 \cdot 10^{31}$	5.41 $\cdot 10^{15}\pm 1.24 \cdot 10^{15}$	1.02 $\cdot 10^{15}\pm 2.01 \cdot 10^{14}$	0	0	0
Hyades	5000	5999	11	11	665 $\pm^{13}_{13}$	0.13 $\pm 0.01$	1.9 $\cdot 10^{33}$	-	1.06 $\pm 0.28$	7.75 $\cdot 10^{43}\pm 7.76 \cdot 10^{33}$	-	1.36 $\cdot 10^6\pm 4.59 \cdot 10^5$	0	0	1
Hyades	3500	3749	14	31	665 $\pm^{13}_{13}$	0.13 $\pm 0.01$	8.8 $\cdot 10^{31}$	1.13 $\pm 0.24$	1.16 $\pm 0.20$	1.54 $\cdot 10^{33}\pm 2.27 \cdot 10^{32}$	2.29 $\cdot 10^3\pm 5.82 \cdot 10^2$	2.38 $\cdot 10^4\pm 5.14 \cdot 10^3$	0	0	1

**Table 3.** Summary of activity parameters of all clusters and  $T_{\text{eff}}$  bins in equivalent duration distributions.

cluster	$T_{\text{min}} [\text{K}]$	$T_{\text{max}} [\text{K}]$	$n_*$	$n_{\text{flares}}$	age [Myr]	[Fe/H]	$ED_{\text{min}} [\text{s}]$	$\alpha_B$	$\alpha_{\text{MK}}$	$\beta_2 [\text{yr}^{-1}]$	$\beta_B [\text{yr}^{-1}]$	$\beta_{\text{MK}} [\text{yr}^{-1}]$	$tr_2$	$tr_B$	$tr_{\text{MK}}$	
Pleiades	4000	4999	87	110	$125 \pm^{25}_{25}$	-	$2.3 \cdot 10^1$	$1.68 \pm 0.07$	$1.68 \pm 0.07$	$175.40 \pm 3.06$	$26.23 \pm 1.80$	$26.08 \pm 1.74$	0	0	0	
Pleiades	3000	3249	353	129	$125 \pm^{25}_{25}$	-	$9.1 \cdot 10^2$	$2.26 \pm 0.12$	$2.24 \pm 0.12$	$1663.97 \pm 8.43$	$16801.52 \pm 1988.56$	$14323.95 \pm 1675.01$	0	0	0	
Pleiades	3250	3499	168	185	$125 \pm^{25}_{25}$	-	$2.2 \cdot 10^2$	$2.03 \pm 0.09$	$2.02 \pm 0.09$	$1250.16 \pm 3.32$	$1524.74 \pm 130.65$	$1437.66 \pm 122.52$	0	0	0	
Pleiades	2500	2999	63	28	$125 \pm^{25}_{25}$	-	$2 \cdot 10^2$	$1.40 \pm 0.32$	$1.38 \pm 0.26$	$732.64 \pm 89.39$	$3.07 \pm 0.97$	$2.55 \pm 0.68$	0	1	1	
Pleiades	3750	3999	52	61	$125 \pm^{25}_{25}$	-	$4.6 \cdot 10^1$	$1.86 \pm 0.12$	$1.84 \pm 0.11$	$337.15 \pm 3.77$	$133.53 \pm 15.57$	$118.85 \pm 13.38$	0	0	0	
Pleiades	5000	5999	53	14	$125 \pm^{25}_{25}$	-	$0.02 \pm 0.03$	$4.9$	$1.27 \pm 0.25$	$1.32 \pm 0.17$	$9.24 \pm 1.16$	$0.13 \pm 0.03$	$0.20 \pm 0.04$	1	1	1
Pleiades	3500	3749	50	47	$125 \pm^{25}_{25}$	-	$-0.02 \pm 0.03$	$1.6 \cdot 10^2$	$1.88 \pm 0.11$	$838.25 \pm 8.01$	$338.29 \pm 38.96$	$256.41 \pm 28.27$	0	0	0	
M35	4000	4999	221	7	$149 \pm^{13}_{13}$	-	$-0.21 \pm 0.06$	$5.2 \cdot 10^2$	-	$1.34 \pm 0.76$	$202.70 \pm 21.23$	-	$0.26 \pm 0.20$	1	0	1
Rup 147	5000	5999	39	7	$2301 \pm^{380}_{257}$	-	$0.08 \pm 0.04$	$4.0$	-	$1.95 \pm 0.30$	$3.07 \pm 0.21$	-	$2.58 \pm 0.79$	0	0	0
Hyades	4000	4999	32	22	$665 \pm^{76}_{76}$	-	$0.13 \pm 0.01$	$4.4$	-	$1.13 \pm 0.25$	$30.87 \pm 8.30$	-	$0.05 \pm 0.01$	0	0	1
Hyades	3000	3249	56	14	$665 \pm^{70}_{70}$	-	$0.13 \pm 0.01$	$9.8 \cdot 10^2$	$1.87 \pm 0.60$	$1.78 \pm 0.48$	$1037.31 \pm 28.99$	$316.11 \pm 191.27$	$132.35 \pm 63.88$	0	1	1
Hyades	3250	3499	42	20	$665 \pm^{70}_{70}$	-	$0.13 \pm 0.01$	$5.5 \cdot 10^2$	$1.82 \pm 0.37$	$1.77 \pm 0.30$	$1281.92 \pm 18.75$	$264.94 \pm 97.28$	$156.31 \pm 46.78$	0	1	1
Hyades	3750	3999	5	21	$665 \pm^{70}_{70}$	-	$0.13 \pm 0.01$	$3.9$	$1.46 \pm 0.29$	$1.49 \pm 0.27$	$157.65 \pm 8.25$	$8.37 \pm 2.48$	$10.09 \pm 2.71$	0	1	1
Hyades	5000	5999	11	8	$665 \pm^{70}_{70}$	-	$0.13 \pm 0.01$	$2.4 \cdot 10^1$	-	$1.06 \pm 0.28$	$182.82 \pm 18.30$	-	$0.01 \pm 0.00$	1	0	1
Hyades	3500	3749	14	30	$665 \pm^{70}_{70}$	-	$0.13 \pm 0.01$	$6.5$	-	$1.14 \pm 0.16$	$172.86 \pm 33.54$	-	$0.18 \pm 0.03$	0	0	1

526 West et al. (2015) found that all M1-M4 dwarfs with rotation 527  
 527 periods shorter than 26 days, and all M5-M8 dwarfs with periods 528  
 528 shorter than 86 days show H $\alpha$  emission, indicating their 529  
 529 magnetic activity. 582

530 Assuming a typical binary fraction for early and mid 531  
 531 dwarfs (Fischer & Marcy 1992), we can expect some of the 532  
 532 stars at  $T_{\text{eff}} > 3000$  K to belong to unresolved binary 533  
 533 companions with  $T_{\text{eff}} < 3000$  K. A misattributed flare on an early 534  
 534 dwarf then will be assigned a too small  $ED$ , but still a corr535  
 535  $E_{Kp,\text{flare}}$  because the count ratios are equal to the  $L_{Kp}$  ratios. 587

### 536 5.5. Consistency of Hyades' and Praesepe's results 588

537 HRDs constructed in Gaia Collaboration et al. (2018a) indicate 538  
 538 only slightly older ages for Hyades and Praesepe. We expect our 539  
 539 results to reflect this similarity. 591

540 *Are the samples comparable? Membership determination 593  
 541 differ. Can we frame this as a statistical test, i.e. answer 594  
 542 question: What is the probability that the activity distribution 595  
 543 for both clusters were drawn from the same underlying distribu 596  
 544 tion for a given age and mass bin?* 598

545 Metallicity is controlled for ([Fe/H](Praesepe) = 0.599  
 546 [Fe/H](Hyades) = 0.13, Netopil et al. 2016). 600

### 547 5.6. Consistency of Pleiades and M35 results 604

548 M35 is has subsolar metallicity, while Pleiades are roughly solar. 605

### 549 5.7. Jim's section(s) 606

550 Flaring activity function of mass and age – a gyrochronology 551  
 551 analog? 608

552 Results in the context of Davenport et al. (2019): How well does 553  
 553 the model fit if we have isochronal and not rotational ages 609  
 554 for our stars? 611

555 Davenport et al. (2019) note a sample bias towards more active 556  
 556 stars. Their models overpredicts the superflaring rate of the 614  
 557 erage Sun-like sample from Shibayama et al. (2013) and more 615  
 558 resembles the rate for their most active sub-sample. *Do we see 616  
 559 the same effect in our OC sample? We should not. Or do 617  
 560 our cluster memberships depend on activity?* 618

### 561 5.8. Universality of $\alpha$

562 Taking into account uncertainties and systematic errors resulting 563  
 563 from power law fitting methods, the power law exponent  $\alpha \sim 2$  624  
 564 appears to be the same for all studies on flare statistics so far, 625  
 565 respective of spectral type. A notable exception are A stars 626  
 566 Kepler that follow a power law with  $\alpha \sim 1$  that may indicate 629  
 567 different physical process (Yang & Liu 2019). 630

### 568 5.9. Deviations from single power law 634

569 Spots can survive on the stellar surface from a few days to nearly 570  
 570 a year (Namekata et al. 2017; Davenport 2015). Namekata et al. 571  
 571 (2017) find conceivable that spots evolve on timescale shorter 572  
 572 than the estimated lifetimes. Complex spot geometry is correlated 573  
 573 with the strongest X-class flares on the Sun (Toriumi et al. 574  
 574 2017; Sammis et al. 2000). This support the idea that flares 575  
 575 associated with the presence of certain types of starspots, 576  
 576 more generally, certain types of active regions. Since we can reasonably 577  
 577 expect that there is a maximum flare energy a spot can 578  
 578 produce, the underlying power law relation must break a som579

$ED_{\text{max}}$ . We tested a possible truncation of our FFDs, but find no conclusive evidence for it in any FFD with  $> 50$  data points. As we stack multiple targets, each potentially with multiple, evolving spots of various sizes on their surfaces, into one FFD at a time, we might observe a deviation but no truncation. A different explanation is simply that we do not sample the maximum energies, as extremely high relative fluxes have been observed in the past (Paudel et al. 2018; Jackman et al. 2019; Schmidt et al. 2016).

## 588 6. Summary and Conclusions

589 *Is there or will be there more data available to further extend the 590 sample?*

591 *Acknowledgements.* This work made use of the `gaia-kepler.fun` crossmatch 592 database created by Megan Bedell. Kepler-affiliated tools were used in the process: `lightkurve`, `K2SC`, `AltaiPony`. Also: `numpy`, `pandas`, `astroML`, `astropy`, 593 `specmatch-emp`, `bokeh` (Bokeh Development Team 2019)... `TOPCAT`: This 594 research made use of the cross-match service provided by CDS, Strasbourg. This 595 work has made use of data from the European Space Agency (ESA) mission `Gaia` 596 (https://www.cosmos.esa.int/gaia), processed by the `Gaia` Data Processing 597 and Analysis Consortium (DPAC, https://www.cosmos.esa.int/web/gaia/dpac/consortium). Funding for the DPAC has been provided by national 598 institutions, in particular the institutions participating in the `Gaia` Multilateral 599 Agreement. If you have used `Gaia` DR2 data in your research, please cite both the `Gaia` mission paper and the `Gaia` DR2 release paper: Gaia Collaboration et al. (2016): Description of the `Gaia` mission (spacecraft, instruments, survey and measurement principles, and operations), Gaia Collaboration et al. (2018b): Summary of the contents and survey properties.

## 599 References

- 600 Aarnio, A. N., Matt, S. P., & Stassun, K. G. 2012, ApJ, 760, 9
- 601 Aarnio, A. N., Stassun, K. G., Hughes, W. J., & McGregor, S. L. 2011, Sol. Phys., 268, 195
- 602 Aigrain, S., Parviainen, H., & Pope, B. J. S. 2016, MNRAS, 459, 2408
- 603 Alvarado-Gómez, J. D., Drake, J. J., Cohen, O., Moschou, S. P., & Garraffo, C. 2018, ApJ, 862, 93
- 604 Anders, F., Khalatyan, A., Chiappini, C., et al. 2019, A&A, 628, A94
- 605 Andrae, R., Fouesneau, M., Creevey, O., et al. 2018, A&A, 616, A8
- 606 Bailer-Jones, C. A. L., Andrae, R., Arcay, B., et al. 2013, A&A, 559, A74
- 607 Barentsen, G., Hedges, C., Saunders, N., et al. 2018, arXiv e-prints, arXiv:1810.12554
- 608 Barnes, S. A. 2003, ApJ, 586, 464
- 609 Bauke, H. 2007, European Physical Journal B, 58, 167
- 610 Bessell, M. S. & Brett, J. M. 1988, Publications of the Astronomical Society of 611 the Pacific, 100, 1134
- 612 Bochanski, J. J., Hawley, S. L., Covey, K. R., et al. 2010, AJ, 139, 2679
- 613 Bochanski, J. J., West, A. A., Hawley, S. L., & Covey, K. R. 2007, AJ, 133, 531
- 614 Bokeh Development Team. 2019, Bokeh: Python library for interactive visualization
- 615 Bouy, H., Bertin, E., Barrado, D., et al. 2015, Astronomy and Astrophysics, 575, A120
- 616 Boyajian, T. S., von Braun, K., van Belle, G., et al. 2013, The Astrophysical Journal, 771, 40
- 617 Burgasser, A. J., Cruz, K. L., Cushing, M., et al. 2010, ApJ, 710, 1142
- 618 Burgasser, A. J., Liu, M. C., Ireland, M. J., Cruz, K. L., & Dupuy, T. J. 2008, ApJ, 681, 579
- 619 Burgasser, A. J.,Looper, D. L., Kirkpatrick, J. D., & Liu, M. C. 2007, ApJ, 658, 557
- 620 Burgasser, A. J. & McElwain, M. W. 2006, AJ, 131, 1007
- 621 Burgasser, A. J., McElwain, M. W., Kirkpatrick, J. D., et al. 2004, AJ, 127, 2856
- 622 Candelaresi, S., Hillier, A., Maehara, H., Brandenburg, A., & Shibata, K. 2014, ApJ, 792, 67
- 623 Cantat-Gaudin, T., Jordi, C., Vallenari, A., et al. 2018, A&A, 618, A93
- 624 Carpenter, J. M. 2001, The Astronomical Journal, 121, 2851
- 625 Chambers, K. C., Magnier, E. A., Metcalfe, N., et al. 2016, ArXiv e-prints [arXiv: 1612.05560]
- 626 Chang, S.-W., Byun, Y.-I., & Hartman, J. D. 2015, ApJ, 814, 35
- 627 Chang, S. W., Byun, Y. I., & Hartman, J. D. 2016, VizieR Online Data Catalog, J/ApJ/814/35
- 628 Clarke, R. W., Davenport, J. R. A., Covey, K. R., & Baranec, C. 2018, ApJ, 853, 59

- 648 Cruz, K. L., Burgasser, A. J., Reid, I. N., & Liebert, J. 2004, ApJ, 604, L61 727  
 649 Cruz, K. L., Reid, I. N., Liebert, J., Kirkpatrick, J. D., & Lowrance, P. J. 2012, AJ, 145, 2421 729  
 650 Curtis, J. L., Wolfgang, A., Wright, J. T., Brewer, J. M., & Johnson, J. A. 2013, AJ, 145, 134 731  
 651 Davenport, J. 2015, PhD thesis, University of Washington 732  
 652 Davenport, J. R. A., Covey, K. R., Clarke, R. W., et al. 2019, ApJ, 871, 241 733  
 653 Davenport, J. R. A., Hawley, S. L., Hebb, L., et al. 2014, ApJ, 797, 122 734  
 654 Davenport, J. R. A., Hawley, S. L., Hebb, L., et al. 2014, ApJ, 797, 122 734  
 655 Davenport, J. R. A., Hawley, S. L., Hebb, L., et al. 2014, ApJ, 797, 122 734  
 656 Doi, M., Tanaka, M., Fukugita, M., et al. 2010, AJ, 139, 1628 735  
 657 Doorsselaere, T. V., Shariati, H., & Debosscher, J. 2017, ApJS, 232, 26 736  
 658 Douglas, S. T., Agüeros, M. A., Covey, K. R., et al. 2014, ApJ, 795, 161 737  
 659 Douglas, S. T., Agüeros, M. A., Covey, K. R., et al. 2016, ApJ, 822, 47 738  
 660 Douglas, S. T., Agüeros, M. A., Covey, K. R., & Kraus, A. 2017, ApJ, 842, 829  
 661 Drake, J. J., Cohen, O., Yashiro, S., & Gopalswamy, N. 2013, ApJ, 764, 170  
 662 Filippazzo, J. C., Rice, E. L., Faherty, J., et al. 2015, ApJ, 810, 158 741  
 663 Finkbeiner, D. P., Schlafly, E. F., Schlegel, D. J., et al. 2016, ApJ, 822, 66 742  
 664 Fischer, D. A. & Marcy, G. W. 1992, ApJ, 396, 178 743  
 665 Froning, C. S., Kowalski, A., France, K., et al. 2019, ApJ, 871, L26 744  
 666 Gaia Collaboration, Babusiaux, C., van Leeuwen, F., et al. 2018a, A&A, 616, 10 745  
 667 Gaia Collaboration, Brown, A. G. A., Vallenari, A., et al. 2018b, A&A, 616, 747  
 668 Gao, X. 2018, ApJ, 869, 9 748  
 669 Gao, X. 2018, The Astrophysical Journal, 869, 9 749  
 670 Gizis, J. E. 2013, ApJ, 779, 172 750  
 671 Gonzalez, G. 2016, MNRAS, 459, 1060 751  
 672 Green, G. M., Schlafly, E. F., Finkbeiner, D., et al. 2018, MNRAS, 478, 651 752  
 673 Green, G. M., Schlafly, E. F., Zucker, C., Speagle, J. S., & Finkbeiner, D. P. 2019, arXiv e-prints, arXiv:1905.02734 753  
 674 Hawley, S. L. & Fisher, G. H. 1992, ApJS, 78, 565 755  
 675 Hilton, E. J., West, A. A., Hawley, S. L., & Kowalski, A. F. 2010, AJ, 140, 1402 756  
 676 Howard, W. S., Corbett, H., Law, N. M., et al. 2019a, ApJ, 881, 9 757  
 677 Howard, W. S., Corbett, H., Law, N. M., et al. 2019b, arXiv e-prints, arXiv:1907.10735 758  
 678 Howell, S. B., Sobeck, C., Haas, M., et al. 2014, PASP, 126, 398 759  
 679 Hunt-Walker, N. M., Hilton, E. J., Kowalski, A. F., Hawley, S. L., & Matthews, J. M. 2012, PASP, 124, 545 760  
 680 Ilin, E., Schmidt, S. J., Davenport, J. R. A., & Strassmeier, K. G. 2019, A&A, 622, A133 761  
 681 Jackman, J. A. G., Wheatley, P. J., Bayliss, D., et al. 2019, arXiv e-prints, arXiv:1902.00900 762  
 682 Kerr, G. S. & Fletcher, L. 2014, ApJ, 783, 98 763  
 683 Kirkpatrick, J. D.,Looper, D. L.,Burgasser, A. J.,et al. 2010, ApJS, 190, 100 764  
 684 Kleint, L.,Heinzel, P.,Judge, P.,&Krucker, S. 2016, ApJ, 816, 88 765  
 685 Koch, D. G., Borucki, W. J., Basri, G., et al. 2010, ApJ, 713, L79 766  
 686 Kovács, G., Bakos, G., & Noyes, R. W. 2005, MNRAS, 356, 557 767  
 687 Kowalski, A. F., Hawley, S. L., Wisniewski, J. P., et al. 2013, ApJS, 207, 15 768  
 688 Kretzschmar, M. 2011, A&A, 530, A84 769  
 689 Lecavelier des Etangs, A., Bourrier, V., Wheatley, P. J., et al. 2012, A&A, 543, L4 770  
 690 Loyd, R. O. P., France, K., Youngblood, A., et al. 2018, ApJ, 867, 71 771  
 691 Luger, R., Kruse, E., Foreman-Mackey, D., Agol, E., & Saunders, N. 2018, AJ, 156, 99 772  
 692 Lurie, J. C., Davenport, J. R. A., Hawley, S. L., et al. 2015, ApJ, 800, 95 773  
 693 Mann, A. W., Feiden, G. A., Gaidos, E., Boyajian, T., & von Braun, K. 2015, ApJ, 804, 64 774  
 694 Mann, A. W., Feiden, G. A., Gaidos, E., Boyajian, T., & von Braun, K. 2016, The Astrophysical Journal, 819, 87 775  
 695 Maschberger, T. & Kroupa, P. 2009, MNRAS, 395, 931 776  
 696 Mondrik, N., Newton, E., Charbonneau, D., & Irwin, J. 2019, ApJ, 870, 10 777  
 697 Morin, J., Donati, J. F., Petit, P., et al. 2008, MNRAS, 390, 567 778  
 698 Namekata, K., Sakaue, T., Watanabe, K., et al. 2017, ApJ, 851, 91 779  
 699 Nardiello, D., Libralato, M., Bedin, L. R., et al. 2016, MNRAS, 463, 1831 780  
 700 Olivares, J., Bouy, H., Sarro, L. M., et al. 2019, A&A, 625, A115 781  
 701 Olivares, J., Sarro, L. M., Moraux, E., et al. 2018, A&A, 617, A15 782  
 702 Paudel, R. R., Gizis, J. E., Mullan, D. J., et al. 2018, ApJ, 861, 76 783  
 703 Pecaut, M. J. & Mamajek, E. E. 2013, ApJS, 208, 9 784  
 704 Priest, E. & Forbes, T. 2002, A&A Rev., 10, 313 785  
 705 Queiroz, A. B. A., Anders, F., Santiago, B. X., et al. 2018, MNRAS, 476, 2556 786  
 706 Rayner, J. T., Cushing, M. C., & Vacca, W. D. 2009, ApJS, 185, 289 787  
 707 Rebull, L., Stauffer, J., Bouvier, J., et al. 2016a, Astronomical Journal, 152, 113, bibtext: 2016AJ....152..113R bibtext[eid=113;adsurl=https://ui.adsabs.harvard.edu/abs/2016AJ....152..113R;adsnote=Provided by the SAO/NASA 788  
 708 Astrophysics Data System] 789  
 709 Rebull, L. M., Stauffer, J. R., Bouvier, J., et al. 2016b, AJ, 152, 113 790  
 710 Rebull, L. M., Stauffer, J. R., Hillenbrand, L. A., et al. 2017, ApJ, 839, 92 791  
 711 Reid, I. N. & Hawley, S. L. 2005, New Light on Dark Stars: Red Dwarfs, Low-Mass Stars, Brown Dwarfs, 2nd edn., Springer-Praxis books in astronomy and astrophysics (Berlin ; New York : Chichester, UK: Springer ; Praxis) 792  
 712 Reino, S., de Bruijne, J., Zari, E., d'Antona, F., & Ventura, P. 2018, MNRAS, 477, 3197 793  
 713 Sammis, I., Tang, F., & Zirin, H. 2000, ApJ, 540, 583 794  
 714 Schmidt, S. J. 2014, Mem. Soc. Astron. Italiana, 85, 741 795  
 715 Schmidt, S. J., Hawley, S. L., West, A. A., et al. 2015, AJ, 149, 158 796  
 716 Schmidt, S. J., Shappee, B. J., Gagné, J., et al. 2016, ApJ, 828, L22 797  
 717 Schmidt, S. J., West, A. A., Bochanski, J. J., Hawley, S. L., & Kielty, C. 2014, PASP, 126, 642 798  
 718 Schmidts, S. J., West, A. A., Hawley, S. L., & Pineda, J. S. 2010, AJ, 139, 1808 799  
 719 See, V., Jardine, M., Vidotto, A. A., et al. 2017, MNRAS, 466, 1542 800  
 720 Shibayama, T., Maehara, H., Notsu, S., et al. 2013, The Astrophysical Journal Supplement Series, 209, 5 801  
 721 Shibayama, T., Maehara, H., Notsu, S., et al. 2013, ApJS, 209, 5 802  
 722 Skrutskie, M. F., Cutri, R. M., Stiening, R., et al. 2006, AJ, 131, 1163 803  
 723 Soares-Furtado, M., Hartman, J. D., Bakos, G. Á., et al. 2017, Publications of the Astronomical Society of the Pacific, 129, 044501 804  
 724 Tilley, M. A., Segura, A., Meadows, V., Hawley, S., & Davenport, J. 2019, Astrobiology, 19, 64 805  
 725 Toriumi, S., Schrijver, C. J., Harra, L. K., Hudson, H., & Nagashima, K. 2017, ApJ, 834, 56 806  
 726 Van Cleve, J. E., Howell, S. B., Smith, J. C., et al. 2016, PASP, 128, 075002 807  
 727 Vanderburg, A. & Johnson, J. A. 2014, Publications of the Astronomical Society of the Pacific, 126, 948 808  
 728 Vanderplas, J., Connolly, A., Ivezić, Ž., & Gray, A. 2012, in Conference on Intelligent Data Understanding (CIDU), 47 –54 809  
 729 Vinícius, Z., Barentsen, G., Hedges, C., Gully-Santiago, M., & Cody, A. M. 2018 Walkowicz, L. M., Basri, G., Batalha, N., et al. 2011, AJ, 141, 50 810  
 730 Watanabe, K., Shimizu, T., Masuda, S., Ichimoto, K., & Ohno, M. 2013, ApJ, 776, 123 811  
 731 West, A. A., Morgan, D. P., Bochanski, J. J., et al. 2011, AJ, 141, 97 812  
 732 West, A. A., Weisenburger, K. L., Irwin, J., et al. 2015, ApJ, 812, 3 813  
 733 Wheatland, M. S. 2004, ApJ, 609, 1134 814  
 734 Yang, H. & Liu, J. 2019, ApJS, 241, 29 815  
 735 Yang, H., Liu, J., Gao, Q., et al. 2017, ApJ, 849, 36 816  
 736 Yee, S. W., Petigura, E. A., & von Braun, K. 2017, ApJ, 836, 77 817

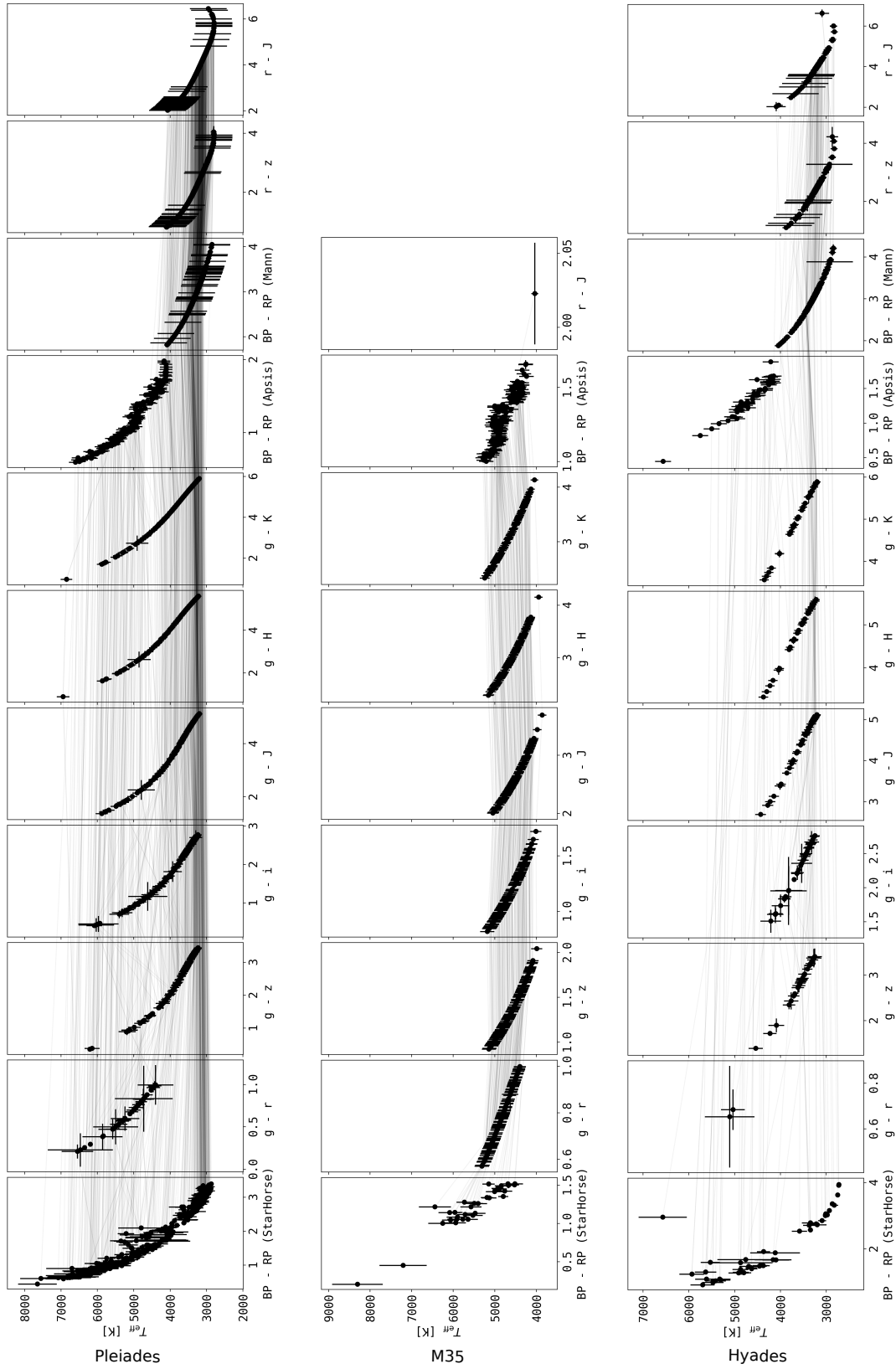


**Fig. 2.** Color-temperature relations for Pleiades, M35, and Hyades.

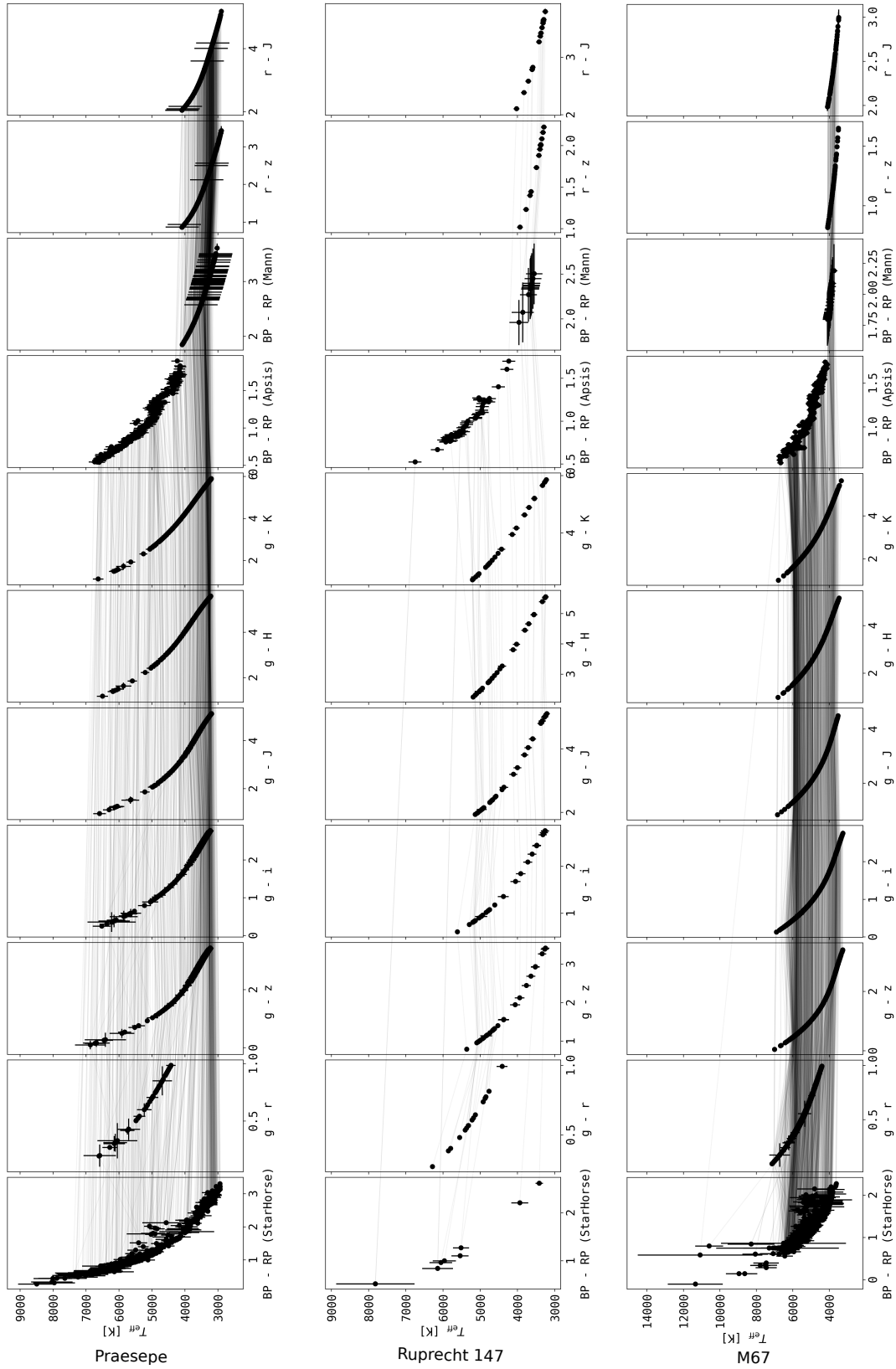


**Fig. 3.** Color-temperature relations for Praesepe, Ruprecht 147, and M67. Description as in Fig. 2.

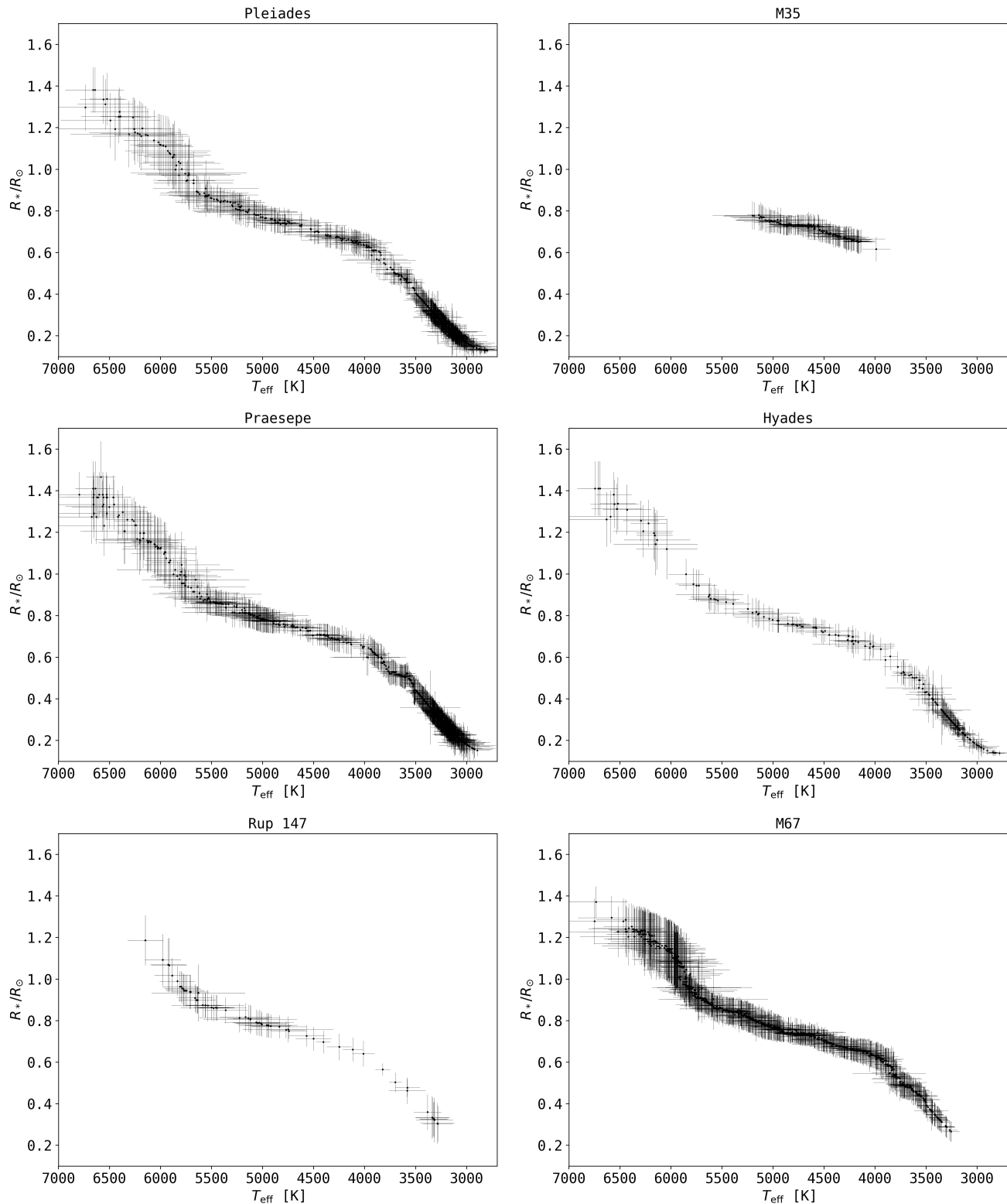


**Fig. 4.**  $T_{\text{eff}}$  –  $R_*$  relation for all clusters in this study.

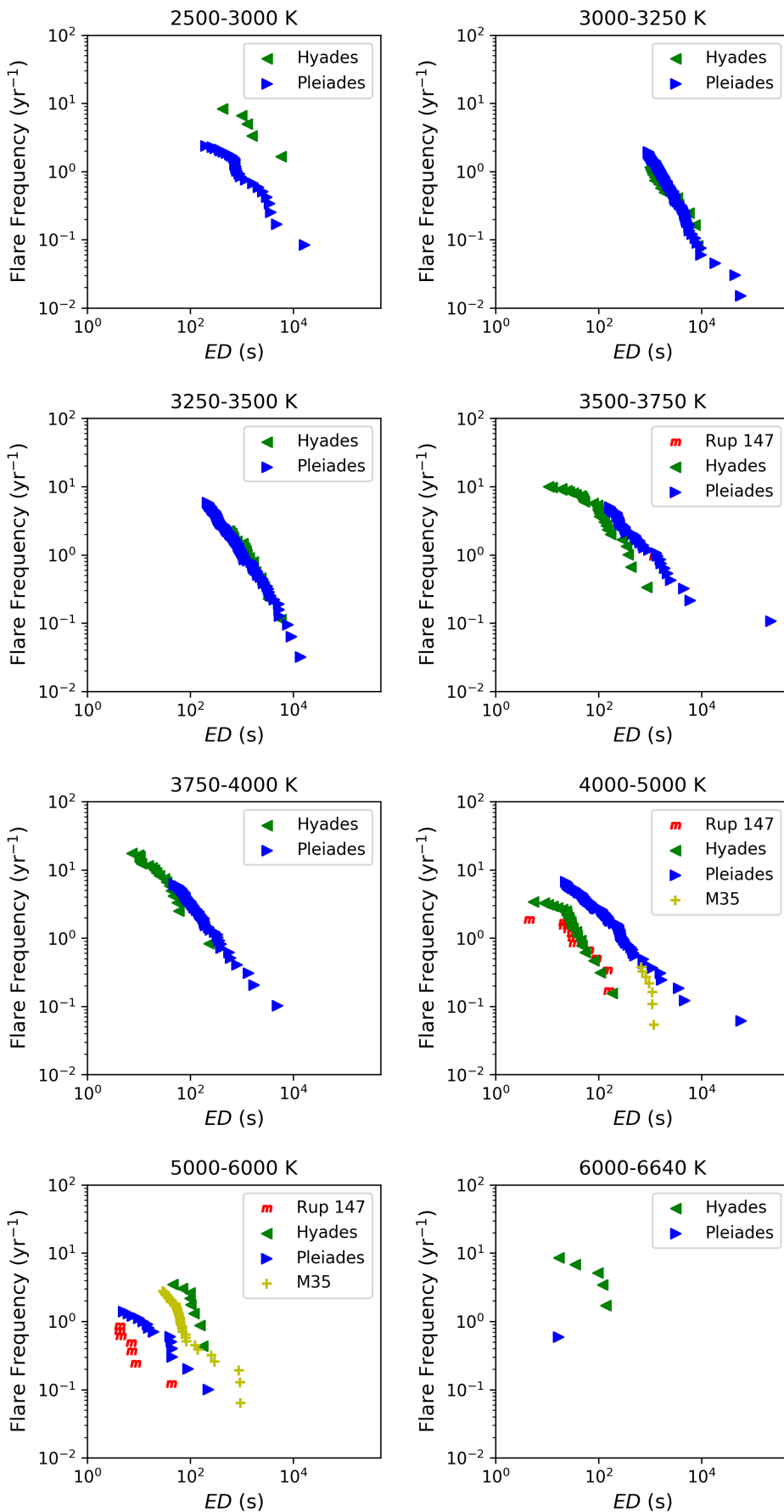


**Fig. 5.** Cumulative flare frequency distributions (FFDs) of equivalent durations ( $ED$ ). In each panel, every distribution belongs to one cluster. The panels are binned by  $T_{\text{eff}}$ .

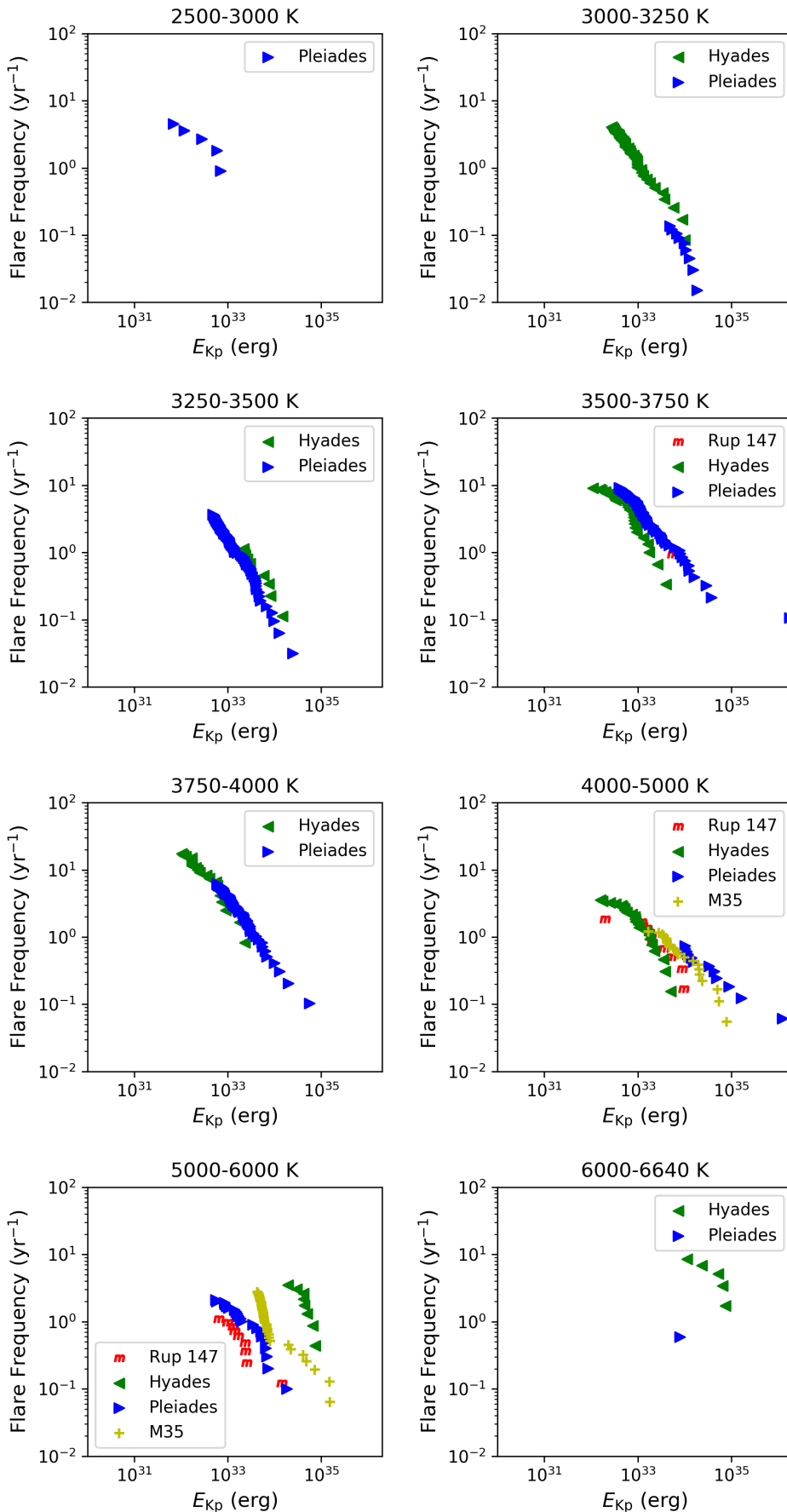


**Fig. 6.** Same as Fig. 5, but of Kepler flare energies  $E_{\text{Kp,flare}}$ .

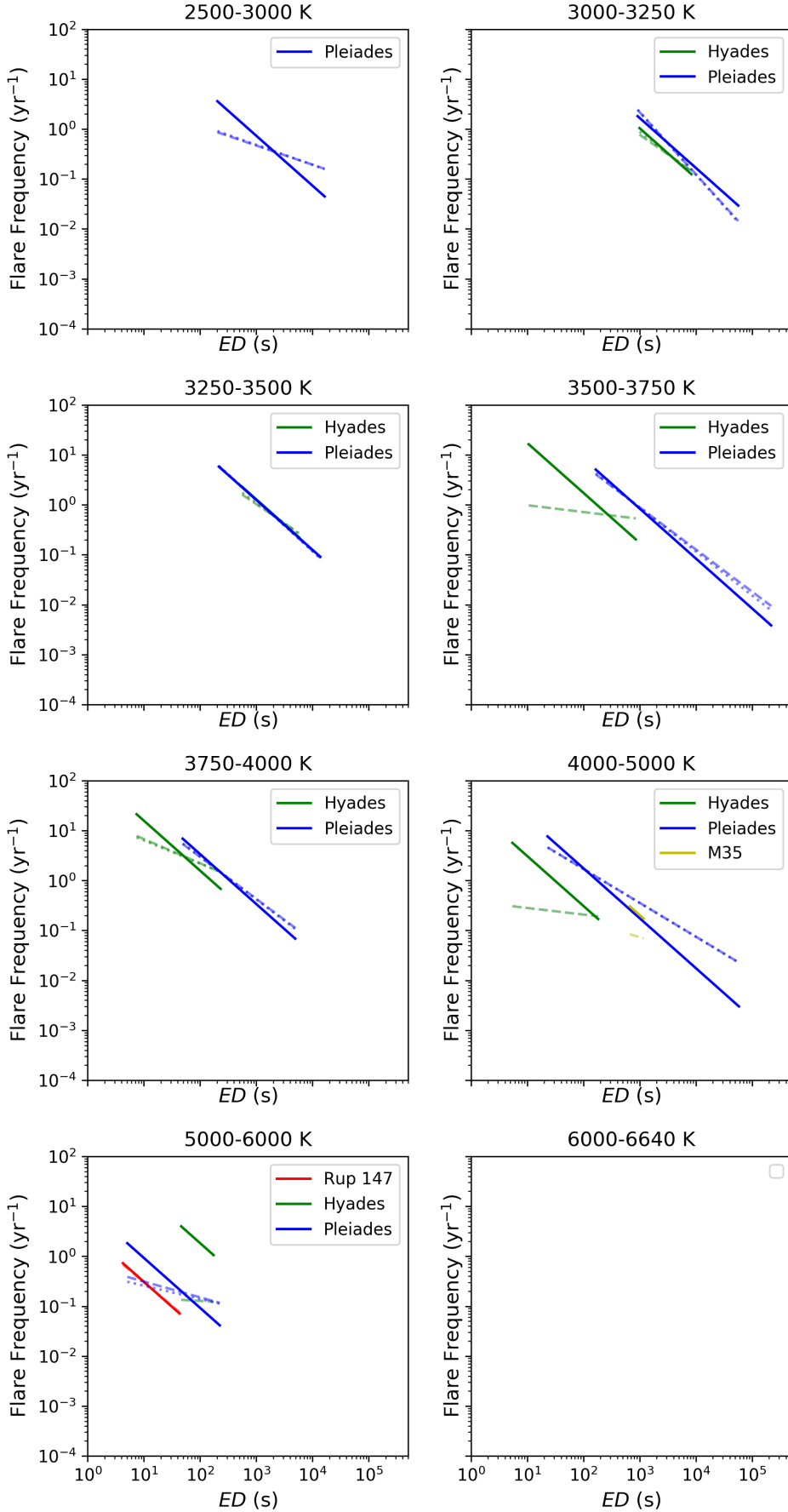


**Fig. 7.** Power law fits to the FFDs of  $ED$  in Fig. 5. Bold line: a power law with  $\alpha = 2$ . Dashed line: best fit parameters were determined following Maschberger & Kroupa (2009) (see Sec. XX). Dotted line: best fit parameters were determined following Bauke (2007) (see Sec. XX)

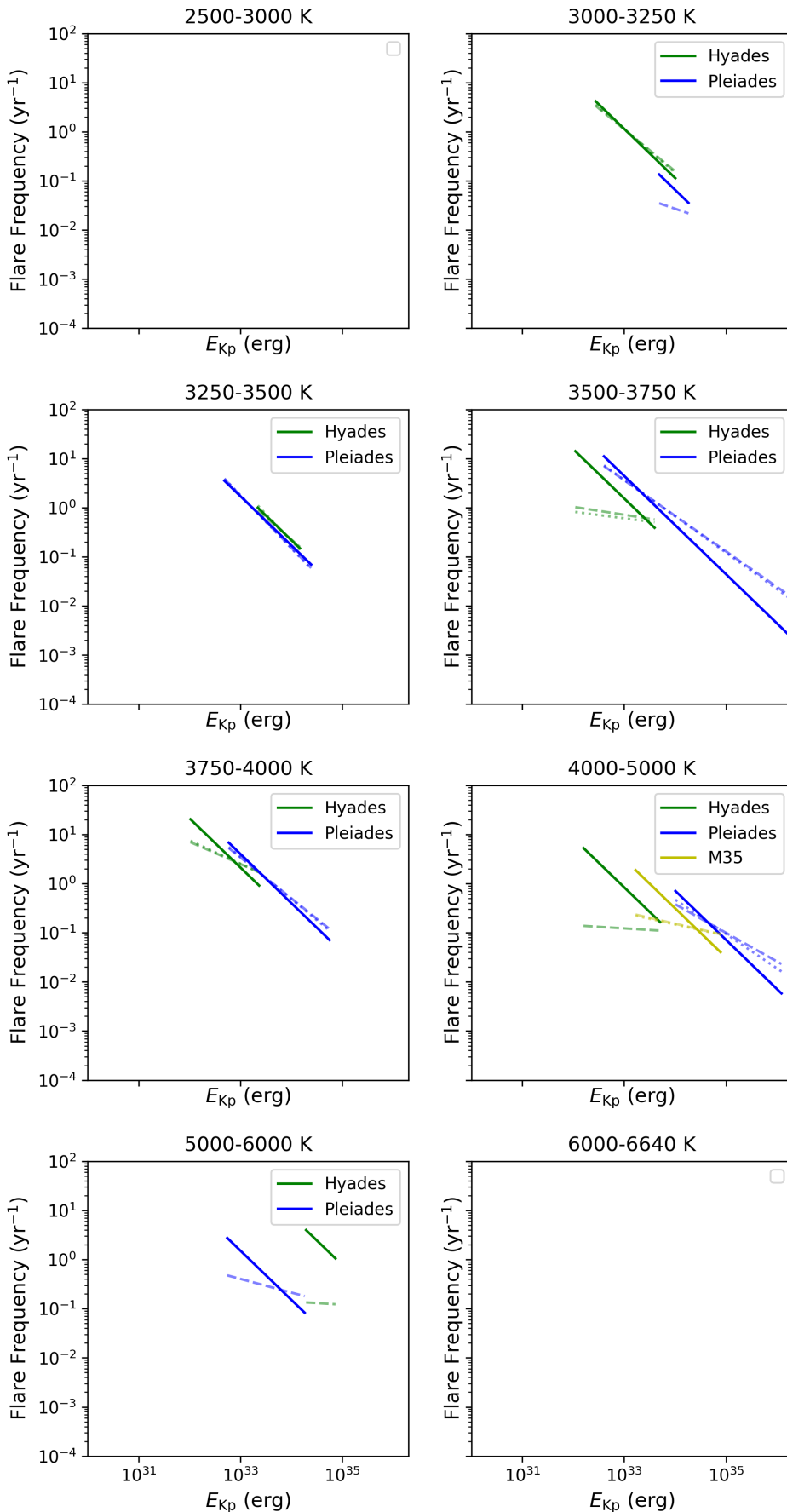


**Fig. 8.** Power law fits to the FFDs of  $E_{Kp,\text{flare}}$  in Fig. 5. See Fig. 7 for details.

## 762 Appendix A: Membership probabilities

763 To match catalogs on RA and declination we used 768  
 764 `astroML.crossmatch` tool for Python (Vanderplas et al. 2012)  
 765 For the studies with classifiers we assigned membership prob795  
 766 bilities as follows. In Gonzalez (2016):

$$\begin{aligned} p(M(\text{member})) &= 0.9, \\ p(BM(\text{binary member})) &= 0.9, \\ p(N(\text{non-member})) &= 0.1, \\ p(SN(\text{single non-member})) &= 0.1, \\ p(BN(\text{binary non-member})) &= 0.1, \\ p(U(\text{unknown member})) &= 0.5. \end{aligned}$$

767 In Curtis et al. (2013):

$$\begin{aligned} p(Y(\text{highest confidence member})) &= 0.9, \\ p(P(\text{possible/probable member})) &= 0.7, \\ p(N(\text{not likely/non-member})) &= 0.7, \\ p(B(\text{photometry consistent with blue stragglers})) &= 0.0. \end{aligned}$$

768 In Rebull et al. (2017):

$$\begin{aligned} p((\text{best})) &= 0.9, \\ p((\text{ok})) &= 0.6, \\ p((\text{else})) &= 0.1. \end{aligned}$$

769 Members from Rebull et al. (2016a); Douglas et al. (2017); and  
 770 Gaia Collaboration et al. (2018a) were assigned  $p = 0.9$  if 769  
 771 appeared in the final catalog. 814  
 772 Table A.1 gives an overview over different membership catalog815  
 773 Figure A.1 shows membership probability histograms of the816  
 774 final sample broken down by membership source. Detailed intro817  
 775 tions on how to reproduce the final sample of members in each  
 776 cluster, and corresponding tables, Python scripts, and Jupyter  
 777 notebooks can be found online<sup>5</sup>

## 778 Appendix B: Cluster parameters

## 779 Appendix C: Broadband photometry: quality cuts 780 and conversions

781 We required `flux/flux_error`  $\geq 10$  for Gaia G, BP, and RP  
 782 bands. We require that the 2MASS measurements for J, H, and  
 783 K to be "A". "A" means that measurements had  $S/N > 10$  and  
 784  $\sigma < 0.11$ . For PanSTARRS photometry, we required that the  
 785 QF\_OBJ\_GOOD quality filter flag was set.  
 786 SDSS and PS1 *ugrizy* bands are similar but not identical, but can  
 787 be converted using Table 2 in Finkbeiner et al. (2016).

## 788 Appendix D: Pixel saturation

789 Resolve different levels of pixel saturation ( $>1$ ,  $>10$ ) and 823  
 790 they contribute to the deviations from the single power law at  
 791 the highest energies.

<sup>5</sup> [https://github.com/ekaterinailin/  
 flares-in-clusters-with-k2-ii](https://github.com/ekaterinailin/flares-in-clusters-with-k2-ii)

## 792 Appendix E: Solar system objects

793 Solar system objects (SSOs) produce brightness excursions in  
 794 K2 light curves that can closely resemble flare signatures. Often,  
 795 they can be distinguished by their symmetric rise and decay  
 796 shape as contrasted with the typical fast-rise gradual decay flare  
 797 shape (Davenport et al. 2014). M. H. Christiansen and colleagues  
 798 developed a routine called SkyBoT that matches positions and  
 799 times to passages of SSOs listed in YYY. RA, declination, start,  
 800 stop, and mid epochs of flares in BKJD are the input parameters.  
 801 We excluded all flare candidates that occurred within X minutes  
 802 of a SSO passage at the star's position. This procedure removed  
 803 ZZ% of all flare candidates. In the case of high energy flares, we  
 804 confirmed the passage by manually inspecting the pixel file with  
 805 the `lightkurve interact` function for TargetPixelFiles.

## 806 Appendix F: Universality of power law exponent $\alpha$

807 We compiled a exhaustive (?) table of previous work where  
 808 power laws were fitted to FFDs using different methods. Table  
 809 F.1 lists the overview. While particular studies consistently find  
 810 values above or below  $\alpha \approx 2$ , the comparison of different studies  
 811 points towards unresolved systematic errors in all these studies.

## 812 Appendix G: Expanding the likelihood

The rate  $\lambda_2$  of flares with energies larger than  $S_2$  is given in  
 Wheatland (2004) as

$$\lambda_2 = \lambda_1 \cdot \left( \frac{S_1}{S_2} \right)^{\alpha-1}. \quad (\text{G.1})$$

$S_1$  denotes the energy above which all flares are detected.  $\lambda_1$  is  
 the corresponding rate.  $\alpha$  remains the power law exponent of the  
 flare frequency distribution.

We are also given the posterior distribution for the rate  $\lambda_2$  of  
 flares above  $S_2$  in Eq. (20) in Wheatland (2004):

$$\begin{aligned} P_2(\lambda_2) &= \int_1^\infty d\alpha \int_0^\infty d\lambda_1 \delta\left(\lambda_2 - \lambda_1 \cdot \left( \frac{S_1}{S_2} \right)^{\alpha-1}\right) \\ &\quad \cdot P_1(\lambda_1) \cdot P_\alpha(\alpha) \end{aligned} \quad (\text{G.2})$$

As we have additional information in the form of uncertainties  
 in our data  $S = \{S_i, \lambda_i, \sigma_{S,i}\}$ , we can expand Eq. G.2 with this  
 knowledge. Assuming that the observed flare energies  $S_i$  with  
 cumulative rates  $\lambda_i$  are distributed around the real flare energies  
 $S_{0,i}$  with Gaussian uncertainties  $\sigma_{S,i}$ , we can define:

$$\begin{aligned} p(S_i|\lambda_1, \alpha, \sigma_{S,i}) &= \frac{1}{2\pi\sqrt{\sigma_{S,i}}} e^{-\frac{(S_i - S_{0,i})^2}{2\sigma_{S,i}^2}} \\ &\quad - \frac{\left( S_i - S_1 \left( \frac{\lambda_i}{\lambda_1} \right)^{-1/(\alpha-1)} \right)^2}{2\sigma_{S,i}^2} \end{aligned} \quad (\text{G.3})$$

We assume in Eq. G.3 that uncertainties on  $\lambda_1$  are negligible. Eq.  
 G.2 then reads:

$$\begin{aligned} P_2(\lambda_2) &= \int_1^\infty d\alpha \int_0^\infty d\lambda_1 \delta\left(\lambda_2 - \lambda_1 \cdot \left( \frac{S_1}{S_2} \right)^{\alpha-1}\right) \\ &\quad \cdot P_1(\lambda_1) \cdot P_\alpha(\alpha) \cdot P_S(S|\lambda_1, \alpha, \sigma_S) \end{aligned} \quad (\text{G.4})$$

**Table A.1.** Membership catalogs overview. No distance are given for Hyades we adopted individual distances for all members.

source	type	clusters covered	notes
Curtis et al. (2013)	classifier	Rup 147	
Douglas et al. (2014)	probability	Hyades, Praesepe	meta study
Bouy et al. (2015)	probability	M35	DANCe
Gonzalez (2016)	classifier	M67	
Rebull et al. (2016a)	members list	Pleiades	meta study
Rebull et al. (2017)	classifier	Praesepe	meta study
Douglas et al. (2017)	members list	Praesepe	meta study
Gaia Collaboration et al. (2018a)	members list	Hyades, M35, Rup 147, Pleiades, Praesepe	Gaia DR2, (1)
Cantat-Gaudin et al. (2018)	probability	M35, Rup147, Pleiades, Praesepe	Gaia DR2
Gao (2018)	probability	M67	Gaia DR2
Reino et al. (2018)	probability	Hyades	Gaia DR1, (1)
Olivares et al. (2018)	probability	Pleiades	Gaia DR2, DANCe
Olivares et al. (2019)	probability	Rup 147	Gaia DR2, DANCe

**Notes.** DANCe: DANCe membership study project. (1) Positions for Hyades were propagated to epoch 2000 using Gaia proper motions.

with

$$P_S(S|\lambda_1, \alpha, \sigma_S) = C \prod_{i=1}^M p(S_i|\lambda_1, \alpha, \sigma_{S,i}). \quad (\text{G.5})$$

825  $C$  absorbs the normalization, or evidence term.

826 Following Wheatland (2004), we marginalize over  $\lambda_1$  using the  
827  $\delta$  function in G.4 to obtain

$$\begin{aligned} P_2(\lambda_2) &= \int_1^\infty d\alpha \cdot P_1\left(\lambda_2 \cdot \left(\frac{S_2}{S_1}\right)^{\alpha-1}\right) \cdot P_\alpha(\alpha) \\ &\cdot P_S\left(S|\lambda_2 \cdot \left(\frac{S_2}{S_1}\right)^{\alpha-1}, \alpha, \sigma_S\right) \end{aligned} \quad (\text{G.6})$$

828 Transforming  $P_S$  into a function of  $\epsilon$  with  $\lambda_1 = -\ln(1-\epsilon)/\Delta T$   
829 yields:

$$\begin{aligned} P_S(S|\epsilon, \alpha, \sigma_S) &= C \prod_{i=1}^M p(S_i|\epsilon, \alpha, \sigma_{S,i}) \\ &= \frac{C}{\Delta T(1-\epsilon)} \\ &\cdot \prod_{i=1}^M \left[ \frac{1}{2\pi\sqrt{\sigma_{S,i}}} e^{-\frac{\left(S_i - S_2 \left(\frac{-\ln(1-\epsilon)}{\Delta T\lambda_i}\right)^{1/(\alpha-1)}\right)^2}{2\sigma_{S,i}^2}} \right] \end{aligned} \quad (\text{G.7})$$

830 Finally,  $P_S$  enters the joint posterior distribution from Eq. 2, that  
831 becomes

$$\begin{aligned} p(\epsilon, \alpha) &= C \cdot (-\ln(1-\epsilon)^M) \\ &\cdot (\alpha-1)^M \cdot \Gamma(\alpha) \left[ \frac{(S_2/S_1)^{M+1}}{\pi} \right]^\alpha \\ &\cdot (1-\epsilon)^{(T/\Delta T) \cdot (S_2/S_1)^{\alpha-1}-1} \\ &\cdot P_S(S|\epsilon, \alpha, \sigma_S). \end{aligned} \quad (\text{G.8})$$

**Table B.1.** Non-exhaustive literature overview over OC parameters.

cluster	source	distance [pc]	age [Myr]	[Fe/H]
<b>M35</b>	<b>adopted in this work:</b>	861	$147.5 \pm^{13.5}_{13.5}$	$-0.21 \pm 0.10$
M35	Bossini et al. (2019) <sup>a</sup>		$402.7 \pm^{13.5}_{0.9}$	
M35	Cantat-Gaudin et al. (2018)	861		
M35	Netopil et al. (2016)			-0.21
M35	Scholz et al. (2015)	830	151	
M35	Geller et al. (2010)		133	
M35	Meibom et al. (2009)		$147.5 \pm^{13.5}_{13.5}$	
M35	Bragaglia and Tosi (2006)	912		
M35	Steinhauser and Deliyannis (2004)			$-0.143 \pm 0.014$
M35	Barrado (2001)		180	
M35	Barrado et al. (2001)			$-0.21 \pm 0.10$
M35	Sung and Bessel (1999)	832		
<b>Rup 147</b>	<b>adopted in this work:</b>	305	$2650 \pm^{380}_{380}$	$0.08 \pm 0.07$
Rup 147	Bragaglia et al. (2018)			$0.08 \pm 0.07$
Rup 147	Cantat-Gaudin et al. (2018)	305		
Rup 147	Gaia Collaboration (2018)	309	$1995 \pm^{404}_{257}$	
Rup 147	Torres et al. (2018)	283	$2650 \pm^{380}_{380}$	
Rup 147	Curtis (2016) <sup>b</sup>			$0.10 \pm 0.02$
Rup 147	Scholz et al. (2015)	270	1953	
Rup 147	Curtis et al. (2013)	300	$3125 \pm^{125}_{125}$	$0.07 \pm 0.03$
<b>Pleiades</b>	<b>adopted in this work:</b>	135.6	$135 \pm^{25}_{25}$	$-0.037 \pm 0.026$
Pleiades	Bossini et al. (2019) <sup>a</sup>		$86.5 \pm^{2.4}_{2.4}$	
Pleiades	Cantat-Gaudin et al. (2018)	135.6		
Pleiades	Gossage et al. (2018)		$135 \pm^{25}_{25}$	
Pleiades	Yen et al. (2018)	126.3	$141.3 \pm^{170}_{100}$	
Pleiades	Chelli and Duvert (2016)	139		
Pleiades	Netopil et al. (2016)			-0.01
Pleiades	Dahm (2015)		$112 \pm^{5}_{5}$	
Pleiades	Scholz et al. (2015)	130	120	
Pleiades	Conrad et al. (2014)			$-0.037 \pm 0.026$
Pleiades	Melis et al. (2014)	136		
Pleiades	Bell et al. (2012)	135	125	
<b>Praesepe</b>	<b>adopted in this work:</b>	185.5	$750 \pm^{3}_{3}$	0.16
Praesepe	Bossini et al. (2019)		$750 \pm^{3}_{7}$	
Praesepe	Cantat-Gaudin et al. (2018)	185.5		
Praesepe	Gossage et al. (2018)		590	
Praesepe	Yen et al. (2018)	183	$794 \pm^{253}_{269}$	
Praesepe	Netopil et al. (2016)			0.16
Praesepe	Scholz et al. (2015)	187	832	
Praesepe	Boesgaard et al. (2013)			0.12
Praesepe	Boudreault et al. (2012)	160	630	
Praesepe	Salaris et al. (2004)	175	650	
<b>M67</b>	<b>adopted in this work:</b>	908	$3639 \pm^{17}_{17}$	$-0.102 \pm .081$
M67	Bossini et al. (2019)		$3639 \pm^{17}_{17}$	
M67	Netopil et al. (2016)			0.03
M67	Scholz et al. (2015)		$3428 \pm^{147}_{72}$	
M67	Conrad et al. (2014)			$-0.102 \pm .081$
M67	Dias et al. (2012)	908	4300	
M67	Oñehag et al. (2011)	880	4200	0.02
<b>Hyades</b>	<b>adopted in this work:</b> <sup>c</sup>		$690 \pm^{160}_{100}$	$0.13 \pm 0.02$
Hyades	Gaia Collaboration (2018)		$690 \pm^{160}_{100}$	
Hyades	Gossage et al. (2018)		680	
Hyades	Liu et al. (2016)			$\pm 0.02$
Hyades	Netopil et al. (2016)			0.13
Hyades	Taylor and Joner (2005)			$0.103 \pm 0.008$
Hyades	Cummings et al. (2005)			$0.146 \pm 0.004$
Hyades	Salaris et al. (2004)		650	0.15
Hyades	Perryman et al. (1998)		$625 \pm^{50}_{50}$	
Hyades	Martin et al. (1998)		$650 \pm^{70}_{70}$	

Article number, page 20 of 22  
**Notes.** <sup>(a)</sup> Bossini et al. (2019) noted some caveats for their determination of ages of young clusters, for which they used Gaia DR2 photometry for isochrone fitting. <sup>(b)</sup> Curtis (2016) reanalysed HIRES spectra using an improved spectroscopic method as compared to Curtis et al. (2013). <sup>(c)</sup> We did not adopt a mean value for the Hyades distance because the cluster members are on average closer than 50 pc.

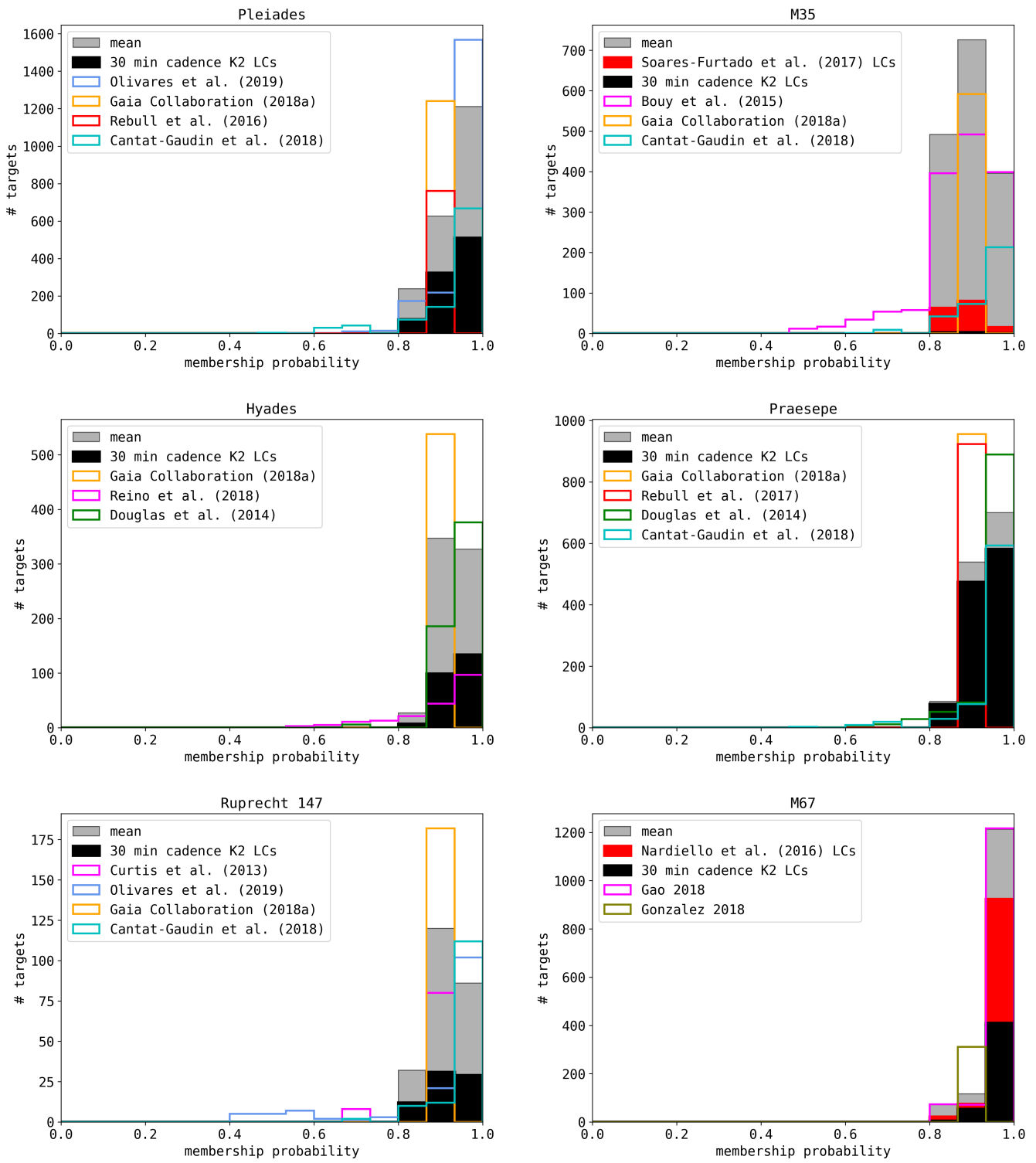


**Fig. A.1.** Membership histograms.

**Table F.1.** Literature overview over power law fitting approaches to FFDs.

Who	method	data	$\alpha - 1$
Hawley et al. (2014)	LSq with Poisson uncertainty, increase the low energy limit until the fit is robust		.95 (binned), 1.01 (cumulative)
Davenport (2016)	weighted LSq, asymmetric Poisson confidence intervals following Gehrels1986		
Gizis (2017)	de-biased MLE (Arnold2015), weight each point with $\text{sqrt}(N)$ in each bin (Clauset+2009)	22 flares on one M7 UCD	.6-1. (31-33 erg)
Paudel et al. (2018)	ML from a paper in 2010, used emcee (Foreman-Mackey2013)		
Lacy (1976)	graphical, linear LSq	386 flares on UV Cetis	.43-1.
Güdel et al.(2003)	-		
Davenport et al. (2012)	Fit $\log_{10} Y = \alpha + (\beta \log_{10} X)(10 - \gamma/(X + \delta))$	~50,000 M dwarfs from SDSS and 1321 M dwarfs from 2MASS	.9-2.1
Lurie et al. (2015)	Bayesian Markov chain Monte Carlo based algorithm (Kelly 2007) for linear regression	2 dMe5 dwarfs	.92-1.03
Audard et al. (2000)	Crawford+1970 MLE (Jauncey-style)	EUVE 12 F-M type stars, 10-20 flares each	.46-1.61
Shakhovskaia (1989)	linear representation, power laws from Gershberg/Shakhovskaya1983	30-40 dK0-dM8, 200 flares	.4-1.4
Yang et al. (2017)	binned FFDs	103187 flares on 540 M-type dwarfs in Kepler	1.07 +/- 0.35
Howard et al. (2018)	fit a cumulative power law, MCMC for uncertainties	575 flares on 284 stars	0.84-1.34
Hilton et al. (2011)			.63-.83